The Marcellus Disappearing Lake

The contribution of surface runoff to two flooding events in 2010

K. van der Hoorn
In cooperation with K.R. Berendsen
Supervisor UU: Dr. M. van der Perk
Supervisor SUNY: P.L. Richards
June 2010

Department of Physical Geography
Faculty of Geosciences
Universiteit Utrecht

Department of Earth Sciences
State University New York
Brockport, New York, USA

Abstract

The karst-related flooding of a valley called Disappearing Lake in New York State, USA has posed a threat to the valley's inhabitants and their properties. Though previous studies have focused on this phenomenon, mechanisms behind the flooding are unknown. Theories have been posted that surface water runoff in combination with other quickflow components and groundwater upwelling contribute to the floods. The fact that floods occur in winter and spring suggests a relation with snowmelt. For this research, a rainfall-runoff model that handles interception, infiltration and depression storage is constructed to quantify the surface runoff component. Two flooding events in January and March 2010 are simulated assuming impermeable conditions for the floodplain, swamps and urban areas. Resulting cumulative runoff volumes show that only 5% of the flood can be contributed to surface runoff. When the floodplain and swamps areas are modelled as unsaturated, the contribution drops below 1%, meaning that the majority of the surface runoff is saturated overland flow. These relatively small runoff contributions could be attributed to high measured values for the saturated hydraulic conductivity. These high values explain the insensitivity of the model to changes in infiltration related parameters. The flooding of the Disappearing Lake does not appear to be surface runoff driven. Other sources of water play a more important role in this phenomenon. Though a high water table appears to be a criterion for floods to occur, further research is necessary to determine the role of groundwater upwelling or other quickflow processes.

Preface

This thesis is the end product of the Hydrology MSc research followed at Utrecht University. The preparation, fieldwork and analysis of the results have been conducted in cooperation with Koen Berendsen. We have both been studying the Disappearing Lake phenomenon, but with different research objectives. Chapters 2 and 3 in this thesis have been written in deliberation with Koen. I would like to thank him for all of his help and for the good times we had in Syracuse. I would also like to thank my supervisors Paul Richards from SUNY Brockport and dr. Marcel van der Perk from Utrecht University for their practical help and advice.
Bill and Nadine, thank you for having us at your place and showing us around in Syracuse and the Thousand Islands. We could not have asked for better tenants. Last but not least I would like to thank our car "The puppy" for not breaking down during the nine weeks of commuting and driving us up Whiteface Mountain.

Contents

List of tables

List of figures

1 Introduction

1.1 Background

Karst-related flooding is a problem occurring all over the world. Karstic aquifers are complex and dynamic systems with many factors influencing the rate of water flow through them. Flooding can occur if the drainage path of groundwater in the karstic aquifer is blocked, causing incoming surface runoff to pond. Also, dramatic changes in the water table due to regional groundwater fluctuations can lead to flooding of the overlying landscape. This can pose a threat to the properties and lives of people.
Three types of flooding that are related to karstic aquifers can be distinguished (Zhou, 2006). Recharge related flooding occurs when the infiltration capacity of the limestone aquifer cannot cope with the precipitation rate or discharge rate of an entering stream. Typically this is caused by clogging of the sinkhole, either by eroded material or by landfill waste. Another reason can be that the incoming flux of water is simply too much for the sinkhole to handle, for example during an extreme rainfall event. Secondly, water flow through the aquifer will follow the route of least resistance and will first fill the larger pores and conduits. If the incoming flux of water is large and has filled all the conduits, it will start flowing through the smaller openings. This will decrease the flow velocity through the aquifer and consequently the conveyance capacity of the aquifer. This is called flow related flooding. Thirdly, discharge related flooding occurs when the discharge of groundwater is inhibited by an increase in water level at the discharge point, usually a spring. This is often caused by human or animal interference, for example the building of dams at or near the discharge point.
Previous studies on karst-related flooding have primarily focused on arid and semi-arid areas with bare, impervious slopes. These slopes enhance runoff production leading to a large surface runoff contribution to flooding. In addition, lake level fluctuations in karst lakes in Croatia are a function of infiltration rates rather than a manifestation of a varying water table (Petrik, 1965). In contrast, Phantom Lake in Pennsylvania, USA lies within a humid area and has no surface streams in or out the basin. Lake level fluctuations must originate from upwelling water of subsurface sources (Wilshusen, 1976).
The annual erratic flooding of a valley called Disappearing Lake in upstate New York, USA occurs under different circumstances. Though the slopes are steep, they are fully covered by forest. In addition, the climate is relatively wet. Furthermore, there are several streams flowing into the basin, but none flow out. The fact that flooding events occur in winter and spring suggests a relation with snowmelt whereas arid regions have increased rainfall as a driving factor. Besides surface water runoff, groundwater could play a key role in the flooding at this site. A previous study by Simons and Voortman (2009) in the same region, but at a smaller scale, showed that groundwater could have as much as a 46% share in a flooding event. An undergraduate study on the Disappearing Lake by Proett (1978) did not have the technical advantages of today's techniques to clarify the mechanisms behind the flooding. Nonetheless, it suggests the flooding is caused by a combination of increased runoff and groundwater upwelling. Another study performed at this site by the US Geological Survey was focused on the residence time of the water in the karstic aquifer and where it eventually discharges. They have conducted tracer studies with dye and plastic balloons but without any conclusive results at the location of the discharge point.
Reports from the valley's inhabitants note that the valley floods at least a couple of times each year but no records are kept by the Town of Marcellus. Other eyewitness reports note that the lake makes gurgling noises as it drains overnight.
Measures that had to be taken against the flooding of the valley have cost the town of Marcellus tens of thousands of dollars. The main road running through the valley had to be placed higher up the hill to prevent it from flooding. Local residents have also raised their

own homes or moved out of the valley. In addition, there is an ongoing dispute between the Town of Marcellus and a resident living close to the sinkhole about who is to blame for the flooding. Many inhabitants blame a former landfill, situated 200 m from the sinkhole, to have clogged the drainage path of the water.
The installation of a pump next to the sinkhole in 1978 has reduced the danger to the valley's inhabitants and their properties. The pump switches on when the water level in the valley gets too high; the water is then pumped into Ninemile Creek, a stream flowing 650 m west of the sinkhole. This has only happened twice: in 1994 and 2007. The situation has definitely improved after the installation of the pump, but still a better understanding of this hydrogeological system could prevent future flooding (in other areas) and lead to better knowledge about the mechanisms behind karst-related flooding.

1.2 Problem description

Modelling the hydrogeology of a karstic aquifer is complicated. Defining the hydrogeological catchment requires detailed information about the geology and fracture orientations all around the catchment. Acquiring this information is beyond the capabilities of this study. Instead, the method applied by Simons and Voortman (2009) was adopted. The flooding of the Disappearing Lake area is hypothesized to be a combination of excessive runoff production and groundwater upwelling. To examine this without investigating the hydrogeology of the karstic aquifer, they have quantified the quickflow component, more specifically the surface runoff component. Surface runoff, either as Hortonian overland flow or as saturated overland flow, contributes to the erratic behavior of a flood. Baseflow and groundwater upwelling are not quantified in this research. Therefore, this study will opt to quantify the contribution of surface water runoff to the flooding of the Disappearing Lake. This could give insight into the role of groundwater in the flooding.

1.3 Research objectives

This research focuses on karst related flooding of the Disappearing Lake valley in New York state, USA. The main research goal of this study is to:

- *Quantify the contribution of surface water runoff to two flooding events in 2010.*

A secondary goal of this study is to:

- *Assess the effect of seasonal variability on the model output by conducting a sensitivity analysis on the model parameters.*

1.4 Research approach

In September and October 2009 fieldwork was conducted in the study area to determine the infiltration capacities of the soils in the valley, leading to values for the saturated hydraulic conductivity. These values serve as input for an infiltration model implemented in a rainfall-runoff model that will simulate the generation of surface runoff after a precipitation event. A Monte Carlo simulation is performed to assess the uncertainty of the model and to obtain average values for the amounts of runoff that are generated. Surface runoff volumes will be compared to calculated flood volumes to determine to contribution of surface runoff to a flood. In addition, the sensitivity of the model output to changes in parameter values is assessed. Changing the values of certain parameters according to their seasonal variability can lead to differences in calculated runoff volumes.

1.5 Thesis outline

The next chapter of this thesis focuses on the characteristics of the study area. The physical processes that are simulated in the model and the accompanying parameters as well as the model structure are described in chapter 3. Chapter 4 gives an overview of the methods that were applied. This includes the source of the data, the statistical preparation, the calculation of flood volumes and the selection of a flooding event and accompanying precipitation time series. The resulting input into the model and the model output are presented in chapter 5. Results will be discussed in chapter 6, followed by the conclusions and recommendations for further research in chapter 7.

2 Study area

The study area is situated east of the town of Marcellus in New York State, USA (figure 2.1). The total catchment size is 8,56 km² whereas the size of the main flood site is 0,0704 km². The most significant feature in the catchment is the polje just east of the village of Marcellus. The polje is bordered by steep slopes of about 8-15% covered entirely by forest. Approximately 50 to 60 m higher the slopes decrease and the landscape is dominated by undulating grassland, cropland and patches of forest. The polje's basin floor consists of a bare floodplain, swamps and patches of forest. Other remarkable features are the golf course north of the polje and the former landfill between the polje and the town. The location of the catchment is shown in figure 2.1a. Elevation differences in the catchment are visible in the Digital Elevation Model (DEM) shown in appendix 1.
The main soil texture class in the catchment is silt loam. In the streams discharging into the polje there are channery silt deposits and the polje's basin floor consists of silt deposits from earlier stands of high water. Figure 2.1b shows the first classification based on land use and hydrologic groups. The hydrologic classification has been derived from the US Department of Agriculture (USDA, 2009).

Figure 2.1a Location of the research area

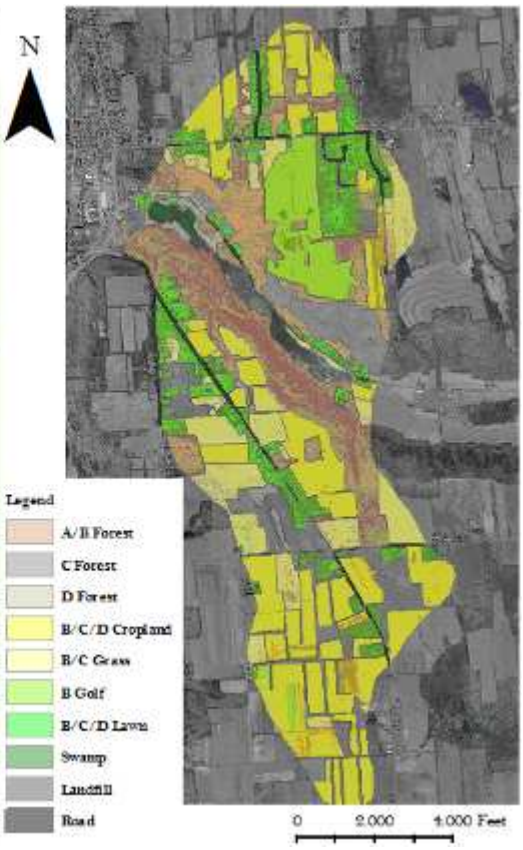

Figure 2.1b Land uses. See paragraph *4.3.2* for further explanation of the classification in the legend.

The geology of the area is dominated by the karstic Onondaga Formation, a Middle Devonian limestone that is present throughout Western New York State (figure 2.2). It also crops out at several places in the streams entering the polje. The formation is also visible at the sinkhole where the water enters the karstic aquifer. The Onondaga Formation is underlain by several dolomite formations with vertical joints that are excellent for groundwater flow. These formations are underlain by the Bertie Formation. This layer consists of shale deposits that impose a barrier for the downward moving groundwater

(Allenson, 1955). Therefore, water originating from the Disappearing Lake will travel no further down through the stratigraphic column than the Bertie Formation, causing it to move laterally. Resting on top of the Onondaga Formation is the Marcellus Formation that consists of shale deposits, comprising the shallow top soil layer in most of the catchment. The contact zone between the Onondaga and Marcellus Formation is visible at several places at the rim of the polje.

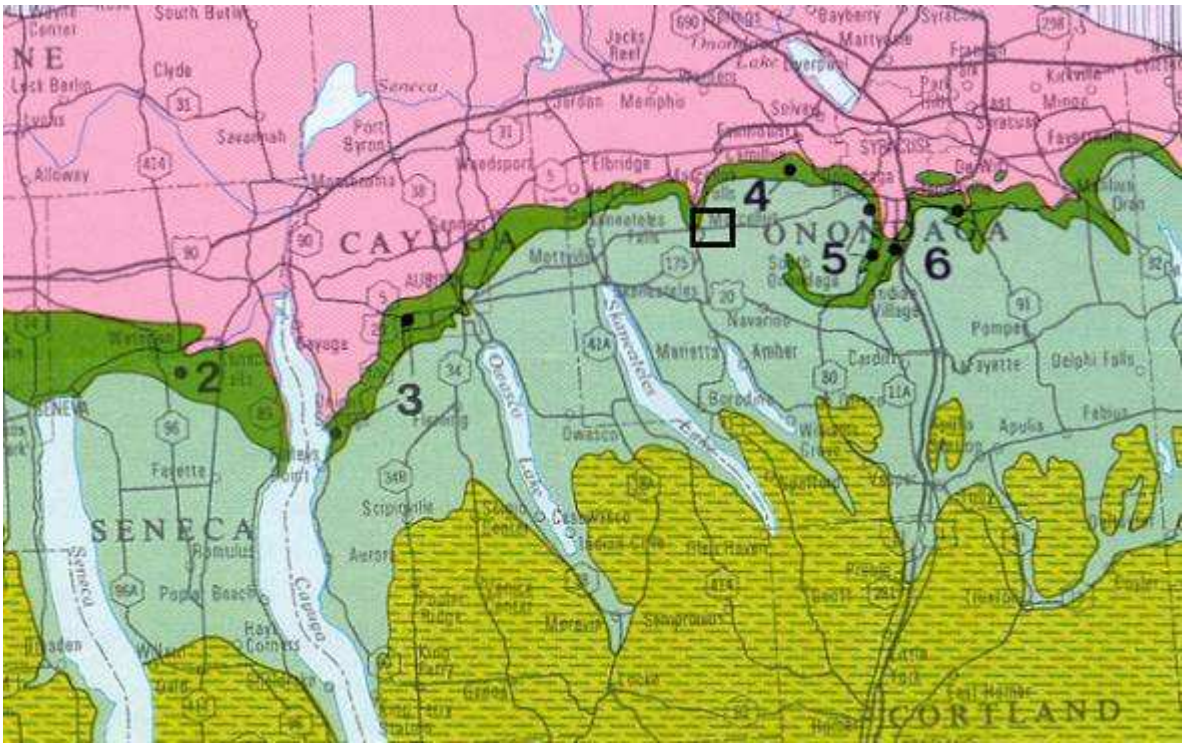

Figure 2.2 The east-west trending Onondaga Formation, shown as the dark green band. The catchment is located in the black square.

The polje occupies the most western portion of the Cedarvale Meltwater Channel. The channel is approximately 15 km long with steep walls bordering the flat basin's floor. It ranges in width from 1.5 km at the outflow point in the southeast to approximately 250 m in the polje's basin in the west. The channel is believed to have been cut during the last stages of glaciation in this area (Fairchild, 1909). Unlike the nearby glacially eroded Finger Lakes and Tully Valley, this channel is cut by meltwater erosion from glacial Lake Warren (Krall, 1966). Presently, the polje contains several alluvial fans protruding into the basin from the larger of the seven inflowing streams. The streams entering the polje are characterized by very steep hillslopes (>20%). The two largest streams show erosive signs of very rapid and violent water movement. Approximately 650 m west of the main flood site runs Ninemile Creek, a northbound flowing creek originating from Otisco Lake and discharging into Onondaga Lake, along which several springs appear. The creek's discharge varies from approximately 0.5 m^3 in summer to 8.5 m^3 in late winter and early spring (Zarrielo, 1999). Previous studies on the hydrogeology of the Disappearing Lake area are scarce. Daniluk et al (2009) proposed that the flooding of the site could be part of a regional phenomena of floodings along the east-west trending Onondaga Formation. However, research on this theory has only been performed at a couple of sites near the towns of Leroy and Caledonia, 150 kilometer to the west (Simons and Voortman, 2009). In the vicinity of Disappearing Lake, no other phenomena of karst-related flooding are reported. The two largest streams discharging into the polje contain outcropping limestone beds of the Onondaga Formation with 5-10 cm wide joints where water enters and re-appears farther down. These fractures

are also visible close to the former landfill. They are probably the only possibility for the water to move downward through the otherwise impermeable limestone. When considering the resurgence of the water that has entered the limestone underlying the polje, Proett (1978) notes that northwest and east-west trending fractures could be possible pathways to low areas along Ninemile Creek. Though Ninemile creek is situated lower than the sinkhole in the Disappearing Lake, there is no apparent surface outlet. Tracer studies performed by the USGS, reported by Proett (1978) suggest that the most likely point of outflow is near Tufa Springs. This is downstream of Marcellus Falls, approximately 4 km downstream from the location of the sinkhole.

The climate in the area is characterized as humid and continental (Peel et al, 2007). The climate is moderated by the Great Lakes, in particular Lake Ontario, resulting in prevailing northwestern winds. When these winds blow over the Great Lakes they enhance the precipitation in the study area, known as lake effect precipitation. This causes Syracuse to receive an average of 294 cm of snow each year. Because the catchment is located in a transition zone between the Ontario lowlands and the Appalachian uplands, the catchment receives additional precipitation from the orographic uplift. The average annual amount of precipitation measured in the nearby Syracuse National Oceanic and Atmospheric Administration (NOAA) meteorological station is 988 mm. Snow is present in the area from October until end of April. Winters are cold with an average temperature in January of -5.7 ºC. Summers are hot with an average temperature in July of 21.3 ºC. Yearly precipitation and temperature trends are displayed in figure 2.3.

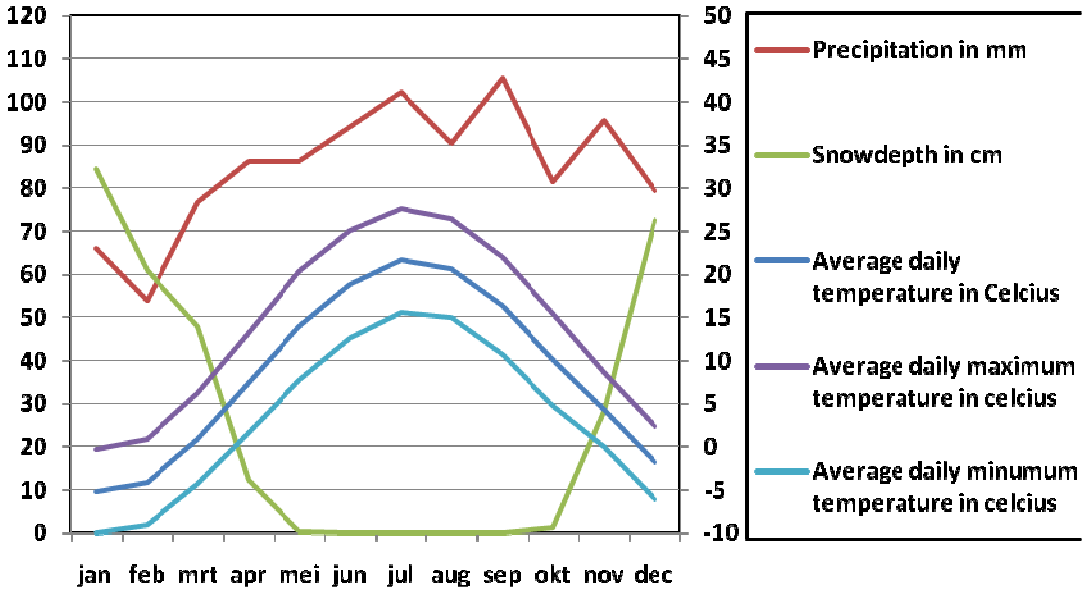

Figure 2.3 Monthly climate data for the catchment area

3 Model description

To simulate flooding events in the Disappearing Lake, a rainfall-runoff computer model was used. The model is based on the European Soil Erosion Model (EUROSEM) (Morgan et al., 1995). It is originally a polygon-, event-based runoff and erosion model, developed for the assessment of soil erosion risk. The hydrological basis of EUROSEM is provided by the KINEROS model developed by Woolhiser (1990). For this study, the adapted PCRaster version of EUROSEM was used. It differs from the original in that it is raster-based and only includes the runoff component, not the erosion processes.
When precipitation enters a catchment different processes control the flow of water before runoff is generated. These processes include interception by vegetation, infiltration and depression storage. Eventually, the excess water flows downstream according to the kinematic water approximation applied in a routing model. The model calculates the cumulative amount of runoff that reaches the outflow point (the sinkhole), runoff hydrographs and graphs of the water fluxes.
The model was implemented in the PCRaster environmental modelling language, which was developed by Utrecht University (PCRaster, 2008). The model uses a raster of 10 by 10 meter. Larger rasters will decrease the slope, affecting the flow velocity and direction of flow. Smaller rasters will increase the computation time and test simulations have proven not to influence the model results. The model runs with timesteps of 30 seconds. Though Simons and Voortman (2009) favour timesteps of 10 seconds to prevent runoff from skipping multiple cells, the model has proven to be not significantly sensitive to this increase in timesteps. Therefore, timesteps of 30 seconds were applied to decrease computation time. In addition, a coarse accuracy test was performed to examine if the model responds logically to changes in parameters.
Because there is a certain degree of randomness in the model, a Monte Carlo simulation was performed. The model was run 200 times to assess its variability and uncertainty in the resulting cumulative runoff.
The processes of interception, infiltration, depression storage and routing and their parameterization are described in the continuation of this chapter.

3.1 Interception

All the water from the precipitation event, rain and snow, is provided to the model in the form of a time series. The time series represents precipitation as a depth of water per timestep. Before reaching the ground, precipitation can strike the vegetation cover. The following formula splits all the precipitation in a part striking the vegetation and a part directly reaching the ground:

$$Int = Rain \cdot COV$$

where Int = the part of the precipitation that is intercepted (m/T), $Rain$ = the total amount of precipitation (m/T) and COV = the percentage of the ground covered by vegetation, depending on vegetation type and land use (-). Consequently, there is a portion of the precipitation that has already reached the ground and a part that is stored on leaves and branches. The intercepted water can only reach the ground as throughfall. Merriam's (1973) approach is that throughfall occurs at the same time as the interception store is filled according to the following formula:

$$IntSt = IntStM\,(1 - e^{-RainCum\,/\,IntStM})$$

where *IntSt* = the depth of water present in the interception store (m), *IntStM* = the maximum interception store (m), *RainCum* = the cumulative amount of rain since the start of the event (m). *IntStM* is defined by Breuer (2003) as the maximum amount of water left on the canopy at the end of a precipitation event under zero evaporation conditions and after drip has stopped. It varies with vegetation type.

3.2 Infiltration

Water passing through the vegetation either as direct rain or as throughfall reaches the ground surface and becomes available for infiltration. EUROSEM as well as a study by Mishra et al (2003) of comparing multiple infiltration models, use the infiltration model of Smith and Parlange (1978) because it performs well on loamy soils, the most abundant soil in the catchment. It uses the cumulative infiltration to calculate the infiltration capacity:

$$Fc = Ksat \frac{e^{Fcum/B}}{e^{Fcum/B} - 1}$$

where *Fc* = the infiltration capacity (m/T), *Ksat* = the saturated hydraulic conductivity (m/T), *Fcum* = the cumulative infiltration since the start of the event (m) and *B* = the saturation deficit parameter (m). The infiltration capacity *Fc* decreases as more water infiltrates and will eventually approach *Ksat*. *B* is a parameter combining the effective capillary drive *G* (m) and the saturation deficit of the soil:

$$B = G(\theta s - \theta i)$$

where θs = the saturated moisture content of the soil (-) and θi = the initial moisture content of the soil (-). The parameter *G* is an integral formulated as:

$$G = \frac{1}{Ksat} \int_{-\infty}^{0} K(\psi) d\psi$$

where $K(\psi)$ = a hydraulic conductivity function and ψ = the soil matric potential (m).
To compensate for rock fragments the *B* term should be adjusted to become the following equation (Woolhiser et al, 1990):

$$Broc = B(1 - ROC)$$

where *Broc* = the adjusted *B* parameter and *ROC* = the rock content of the soil (-). Rocks on the surface can decrease the effective infiltration area of the soil. On the other hand, rocks can increase the infiltration capacity of a soil because they promote the occurrence of macro pores around them. However, there is much uncertainty about this positive effect. Therefore, in this study, this possible positive effect of soil rock content on infiltration capacity was neglected.

3.3 Depression storage

Microdepressions in the soil surface can act as a storage facility for incoming precipitation or water flowing downstream. These depressions can be caused by soil erosion, tree falls and tracks and they can range in size from centimetres to meters. Whereas water falling on a flat surface can either infiltrate immediately or flow downstream as excessive precipitation when

the infiltration capacity is exceeded, water entering depressions can pond. When the water ponds it will increase the residence time of water in the area, reducing the runoff generation. Runoff can only be generated if the storage capacity of the depressions is filled. Although depression storage is discussed frequently in conceptualizations of runoff and infiltration capacity, it has been incorporated as a parameter in relatively few hydrologic models. This study takes the effect of microdepressions into account because it can have a significant effect on runoff production (Richards et al, 2008). In addition, the catchment is densely vegetated. This can have a stabilizing effect on the abundance and shape of microdepressions. In arid regions soil erosion causes the soil surface to be more dynamic which cause the microdepressions to be hard to quantify.

3.4 Routing

Surface water runoff can be modelled either as sheet flow or as channel flow over a local drain direction network created in PCRaster. Sheet flow is characterized by a smaller water depth and lower velocities. Channel flow is characterized by water flow through a stream. The wetted perimeter in sheet flow is represented by the width of a grid cell. The hydraulic radius, the cross-sectional area divided by wetted perimeter, is therefore equal to the water depth. In channel flow, the wetted perimeter is usually assumed to have a trapezoidal shape, but in this study the simplified case of a blocked shaped channel is applied. In this case, the hydraulic radius only depends on the channel width and water depth. The hydraulic radius is used in Manning's equation which relates it to flow velocity, friction slope and Manning's roughness coefficient:

$$V = k\frac{R^{2/3}Sf^{1/2}}{n}$$

where V = the flow velocity (m/s), k = a conversion constant, 1.0 for SI units (s^{-1}), R = the hydraulic radius (m), Sf = the friction slope (-) and n = Manning's coefficient (-).
The flow velocity from Manning's equation is used in the routing model. In this study the model uses the kinematic wave equation that is solved numerically in PCRaster. The principle of the solution is that the incoming and outgoing discharge plus the recharge, in a cell, are related to the water volume in that cell. It is the most simplified version of the Saint Venant equations because it neglects the acceleration and pressure terms that are present in the dynamic wave equation and it assumes the water surface to be equal to the slope of the bottom. Nonetheless, it is accurate enough for the purpose of this research. The kinematic wave equation is made up of the equations of continuity and momentum. The equation of continuity is defined as:

$$q_L + (i - f) = \frac{\partial Q}{\partial x} + \frac{\partial A}{\partial t}$$

where q_L = the lateral inflow (m^2/s), Q = flow (m^3/s), i = rainfall intensity (m^2/s), f = infiltration rate (m^2/s), x = distance in flow direction (m), A = the cross-sectional area (m^2) and t= time (s). After neglecting the acceleration and pressure terms the equation of momentum yields:

$$S_0 = Sf$$

where S_0 = average bottom slope and Sf = the friction slope found in Manning's equation. The combination of the three equations above leads to the routing scheme that is applied in the model.

3.5 Model structure

The flow chart in figure 3.1 shows the connections and interactions between the different components of the model. Precipitation in the form of both snow and rain reaches the surface as direct rain or is intercepted by the vegetation cover. When the maximum interception store is exceeded the intercepted precipitation reaches the surface as throughfall. A small portion of the total precipitation remains in the interception store. When the water reaches the ground it enters the soil according to the infiltration model of Smith and Parlange. Water will infiltrate according to the specific saturated infiltration capacity of a particular land use class. Water becomes excess precipitation when the infiltration capacity is exceeded, but only when the depression storage is filled can the water become runoff. The runoff is then routed downstream over the local drain direction network. Runoff entering a downstream cell where the infiltration capacity or depression storage has not yet been satisfied can infiltrate or be stored in soil depressions again. The assumption was made that if water enters a stream it can no longer infiltrate or be stored; it is directly routed downstream without any loss of water. Precipitation or water coming from upstream cells entering impermeable areas will be modelled as saturated overland flow.
This procedure is simulated for every cell in the catchment and is repeated every time step.

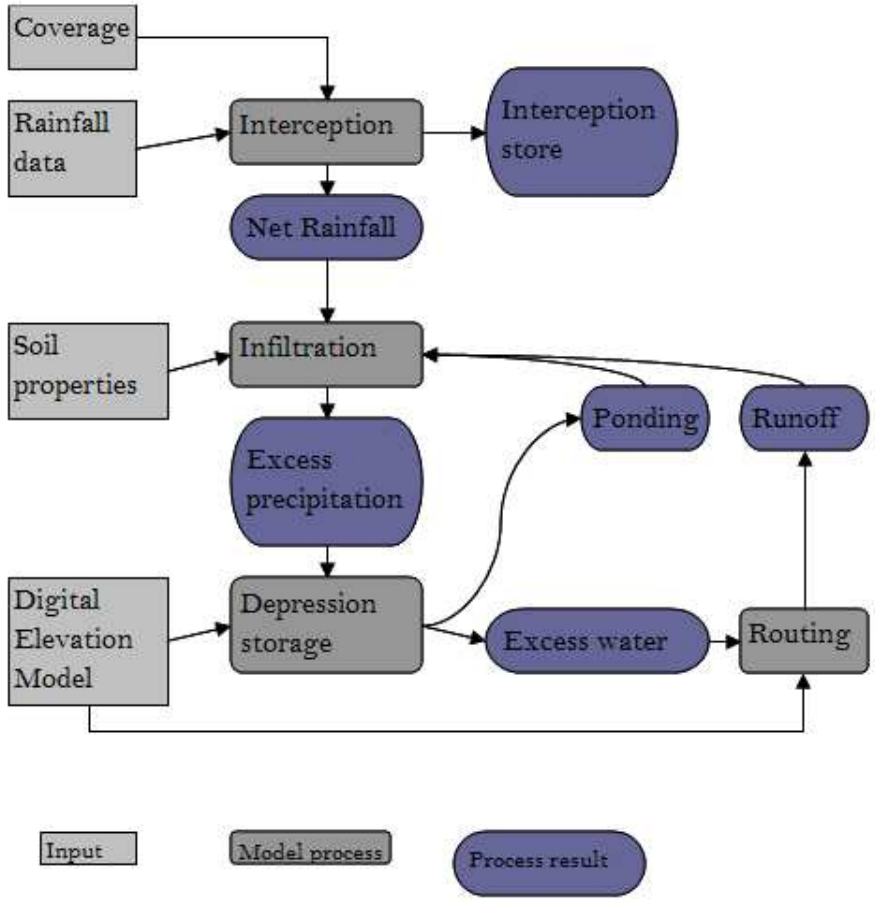

Figure 3.1 Flow chart of the different model processes

4 Model input and model calculation

4.1 Precipitation data

Choosing a precipitation event for a model relies strongly on available data. To relate climate data to the flooding of the polje, information about the lake height is also needed.

4.1.1 Rainfall scenarios

Precipitation data was derived from the nearest NOAA climate station in Skaneateles, situated approximately 8 km from the catchment. The data consists of one measurement per day for both snow depth and rain. This is a very coarse temporal resolution but because there is no tipping bucket installed in the catchment it is the best data available. To convert these daily values to a timeseries with timesteps of 30 seconds a downscaling method can be applied. However, despite the fact that there are many downscaling methods available, most of them are mathematically complex. Therefore, a sensitivity analysis is performed with different rainfall scenarios to examine whether there is a major difference in model output between these scenarios. There is no detailed information available about the intensity and duration of the modelled rainfall events so three scenarios were tested:
1) A *uniform* scenario in which the total volume of rain per day falls over the first twelve hours of the day with a uniform intensity.
2) An *extreme* scenario in which the total volume of rain per day falls in the first four hours and 68% falls within two hours according to a Gaussian distribution.
3) A *normal* scenario in which the total volume of rain per day falls in the first eight hours and 68% falls within four hours according to a Gaussian distribution.
The differences are compared and evaluated. They are discussed in chapter 5.1.

4.1.2 Snowmelt

Besides rainfall, snowmelt is another contributor of water that must be included in the timeseries. Due to lake-effect snowfall events, the catchment area can receive up to 60 cm of snow a day. Modelling snowmelt is challenging because of the course spatial and temporal resolution of the available data, but also because of varying snow density, unknown times of melting and the unknown saturation state of the soil. Regardless of these uncertainties, snowmelt has to be included so assumptions were made. The only available data comes in the form of one value for snow depth per day. This value was converted into a water depth according to the Snow Water Equivalent (SWE). Values for the SWE depend on the type of snow and climate conditions but we assume a ratio of 13:1, meaning 13 cm of snow is equivalent to 1 cm of water (Baxter et al, 2004). Another assumption is that snow melts linearly over the first twelve hours of a day. The linear melting assumption together with the SWE assumption means that if, for example, the snow depth decreases from 40 cm to 30 cm over one day, 10/13 cm of water will be distributed uniformly over the first twelve hours of that day.
The snowmelt was added to the rainfall to give a total precipitation timeseries, under the assumption that snow depth is considered as a layer of water on the surface. Due to a lack of spatial resolution in the precipitation data, the assumption is made that the intensity and amount of precipitation is constant across the entire catchment.
For both types of precipitation we assumed that the soil was saturated.

4.2 Flood data

4.2.1 Selecting flooding events for modelling

At the end of the fieldwork period in October 2009 a pressure transducer was installed in the polje's basin. The transducer was placed one meter deep in floodplain silt deposits, about two meters from the sinkhole. The elevation of the transducer is equal to that of the sinkhole; 197 m in the DEM. This device records, every 30 minutes, the height of the body of water that is on top of it.
Until the transducer had recorded the flooding events of early 2010, modelling was performed on a flooding event of 1994. For this event, climate data was available from the NOAA station but lake level data was scarce. The only available lake heights were daily recordings, read from a story pole, by the Town of Marcellus.
Data from the transducer shows several flooding events occurring between October 2009 and May 2010. Because the temporal resolution of the transducer is much more fine that the recordings from 1994, a selection was made from the events of 2010.
Figure 4.1 shows the transducer data in combination with the available climate data.

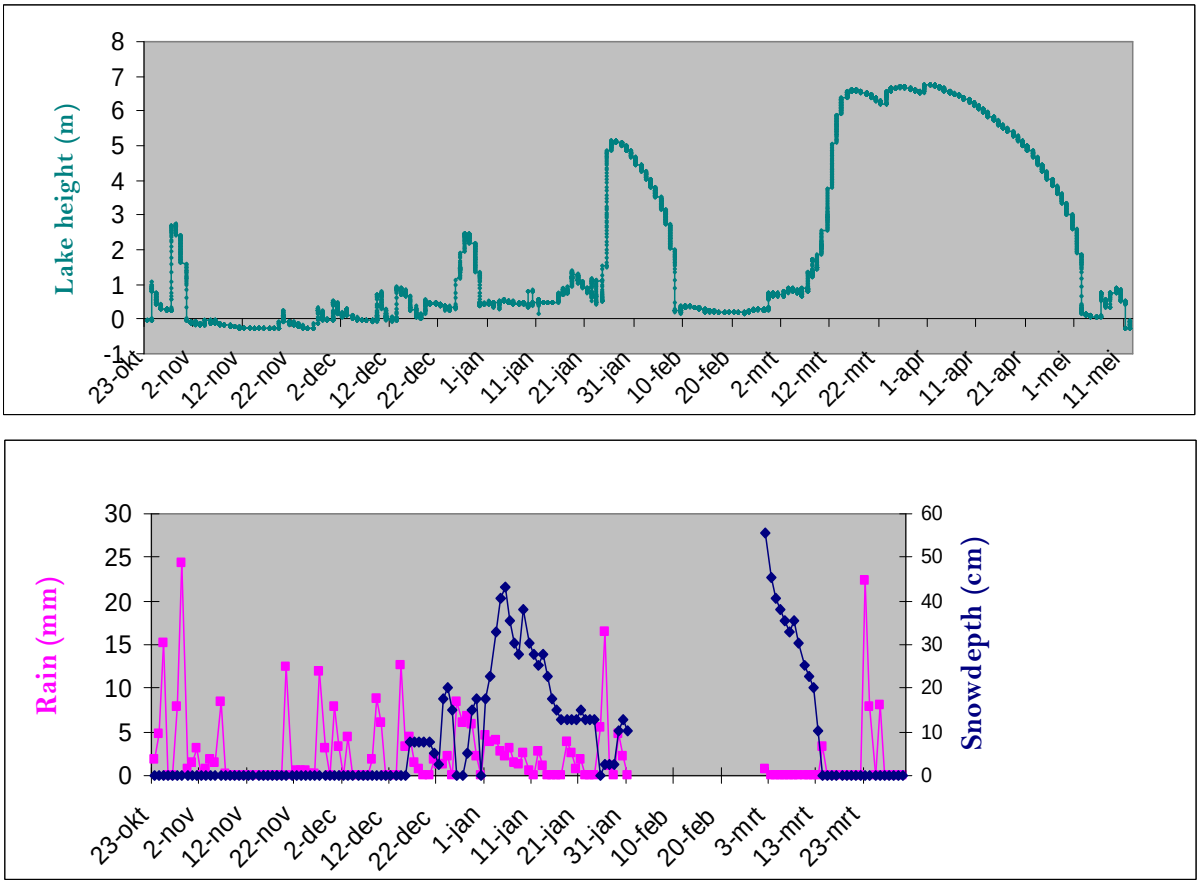

Figure 4.1 Transducer and climate data

The figure shows the relation between precipitation events and the rise of the lake. Smaller events like that of early November 2009 and also small scale fluctuations in lake level in middle December are clearly triggered by (large) rainfall events. Larger flooding events of January 2010 and March 2010 appear to be triggered by a combination of snowmelt and rainfall.
The flooding events that are chosen for this research are those of January 2010 and March 2010. These are the only two events that produce significantly high lake levels and are easy relatable to precipitation events. Smaller events are more difficult to separate from each other. The start of the flood is chosen to be the time the lake starts to rise. The end of the flood is the time the lake reaches its highest point.

The drainage capacity of the sinkhole is assumed to be zero during the rise of the lake because the water table is above the elevation of the sinkhole.

4.2.2 Flood volume calculation

To calculate the contribution of surface water runoff to the two chosen flooding events, the flood volumes have to be known. The flood volume is defined here as the volume of water that is added to the lake between the start of the rise of the lake and the time the lake reaches its highest level. The lake heights at these two moments in time are extracted from the transducer data. In January 2010 a maximum lake height of 5.13 m is observed; in March 2010 the maximum lake height is 6.60 m. These elevations are relative to the elevation of the transducer. The transducer was installed next to the sinkhole which is located in a depression in the floodplain of the polje. The available DEM gives an elevation of 198 m above sea level for the floodplain. The sinkhole was therefore assumed to be at an elevation of 197 m. The lake heights are then, in terms of the elevation in the DEM, at an altitude of respectively 202.13 m and 203.6 m (figure 4.2). PCRaster then calculates the volume of water that is present in the lake at a given lake height according to the topography of the DEM.

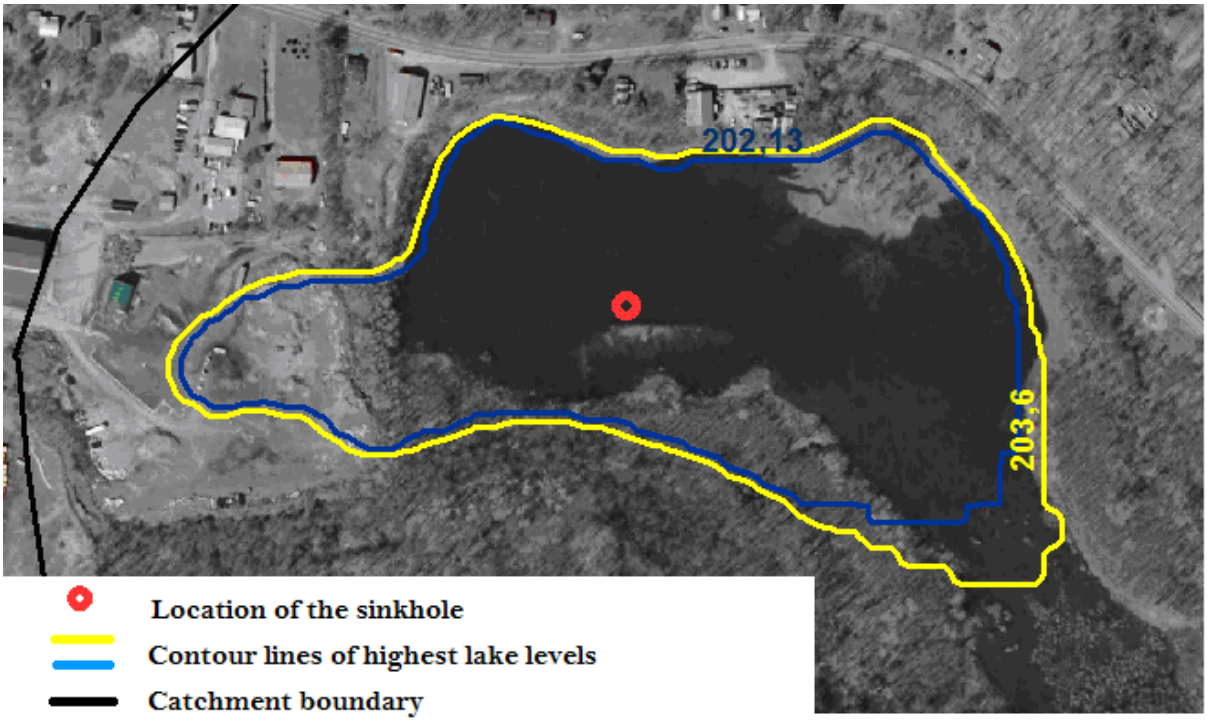

Figure 4.2 Aerial photograph of an earlier flood including contour lines of modelled floods.

However, figure 4.2 shows the topography has changed at the location of the former landfill and in the southeast corner of the lake. At other locations along the flood line of the event visible in the aerial photograph the DEM is not accurate either. Because the DEM is not adapted, other measures are taken to compensate for the flaws in the DEM.
For the purpose of the flood volume calculation (not for runoff modelling), the site of the former landfill was raised to an elevation of 205 m in the PCRaster model, well above the lake level of 203.6 m for the highest modelled flood. The elevated areas at the southern edge of the lake were estimated to compensate for the area in the southeast where there is an extra volume of water that is not included in the contour lines. The area's of both stretches were compared in ArcGIS and are almost equal.

Due to these estimations, the calculation of the flood volumes is not exact. However, the error is expected to be small because the areas of uncertainty are small relative to the bulk of the lake.
When the flood volumes of both events are calculated they are compared to the volumes of precipitation and runoff to extract runoff coefficients and the contribution of runoff to the floods.

4.3 Source and preparation of parameters

This section explains how the data of the model parameters is obtained and how it is analyzed and processed before it can serve as input for the hydrologic model. The saturated hydraulic conductivity and depression storage need to undergo statistical analyses. Other parameters are obtained from literature or are derived empirically. Table 4.1 gives an overview of the model parameters, their units and their source. The parameterization will be described for each process.

Table 4.1 Overview of parameters including source, units and symbols.

Symbol	Name	Source	Unit
ICmax	Maximum interception store	Literature	m
COV	Coverage	Field estimate	-
Ksat	Sat. hydraulic conductivity	Field measurement	m/T
B	Sat. deficit parameter	Empirical derivation	m
ROC	Volumetric rock content	Field estimate	-
G	Capillary parameter	Literature	m
Dst	Depression storage	Field measurement	m
Bw	Channel width	Field estimate/ DEM	m
x	Slope	DEM	-
n	Manning's n	Literature	-

4.3.1 Interception

The parameters that are used in the process of interception are *COV* and *ICmax*.
Values for coverage were estimated at every measurement location as the percentage of vegetation covering the surface area. If more than one type of vegetation is present at a certain location, all the layers of vegetation were taken into account. Measurements were classified according to land use class. Averaging all the values per class results in one number for coverage per class.
The maximum interception store, the maximum depth of water that can be stored on the vegetation's stems and leafs, was taken from the literature. Breuer et al (2003) give an overview of these values for many different types of vegetation. If the exact species of vegetation is not defined in the field or if it is not included in the list, a value for a similar plant of tree was picked.

4.3.2 Infiltration: Ksat

The saturated hydraulic conductivity present in the Smith and Parlange infiltration model was measured in the field. Beforehand, the catchment was divided into different classes based on soil texture, hydrologic group and land use. Soil type, though it effects the saturated hydraulic conductivity value (Fitts, 2002), was quickly removed from the classification because the majority of the catchment consists of silt loam with the exception of some channels and the floodplain, but at these locations no measurements were conducted. The hydrologic classification was derived from the USDA soil data and ranges from A

(potentially high runoff production) to D (potentially low runoff production). Land use is also known to affect saturated hydraulic conductivity values (Yimer et al, 2008).
To avoid bias, measurement locations were randomly generated using ArcGIS software. During the eight weeks of fieldwork, a total of 75 measurements locations were generated where 150 measurements were performed. Two measurements were conducted at each location, approximately 1.5 m from each other, to investigate the spatial distribution of *Ksat*. No measurements were performed in channels, the floodplain in the polje's basin and swamps because they were assumed to be saturated.
Measurements were performed using a double-ring infiltrometer. This device was chosen because it is easy to use, cheap and not significantly less accurate than more expensive and complex equipment. Before the start of a measurement, the soil was wetted to simulate saturated conditions. Next, the double-ring infiltrometer was deployed, water was added every five minutes and at the same time the rate of infiltration was noted. Between 40 and 60 minutes, depending on land use and local soil conditions, the infiltration rate reached a more or less constant level. Figure 4.3 shows a characteristic infiltration curve. Initially the infiltration rate is high (the curve drops) because macropores are being filled and the suction of the soil is strong due to the moisture deficit. Gradually, the curve reaches a constant level indicating the saturated hydraulic conductivity is reached. To obtain a *Ksat* value from this curve, the values at the end of every measurement, when the constant level is reached, were plotted to find the best fit through these points. A trend line was fitted through these points. The average value, given by the slope, represents the saturated hydraulic conductivity. The measurement error in *Ksat* is represented by the deviation from this fit. Because the R^2 value is not always equal to 1, there is some uncertainty in the extracted *Ksat*-value. This error was examined for ten randomly selected measurements.

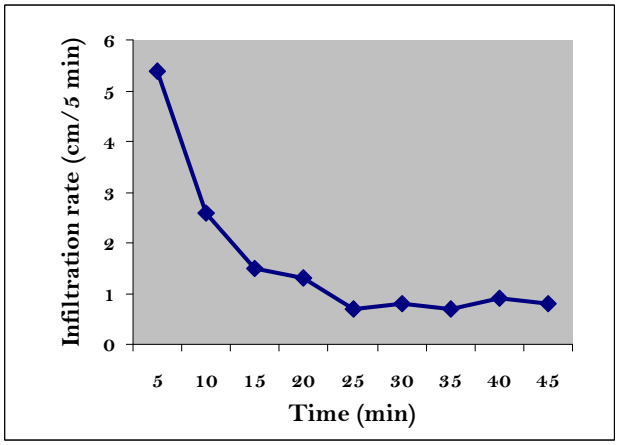

Figure 4.3 Infiltration curve of measurement 2b.

The total of 150 measured *Ksat* values can not be used directly as model input. The data is ordered in classes but statistical tests have to prove if this classification is justified. For the statistical analysis, the method from Bierkens (1994) was applied. First, normality of the data was checked by conducting a Kolmogorov-Smirnov test. If the data was not normally distributed, log tranformation was applied. Secondly, analysis of variance was performed to check if the distinction based on land use and hydrologic group was permitted. Thirdly, F-tests and t-tests were performed to check respectively the equality of variances and equality of means between the different classes. Eventually, these tests can results in the merging of classes if this is desired. Besides statistical results, field interpretations can also affect this.
After the statistical analysis, *Ksat* values were assigned to the (newly defined) classes. In the model, every cell is assigned a value for *Ksat*, depending on which class the cell is in. The way in which this value is assigned depends on the spatial correlation of *Ksat*. A variogram was constructed for each class, using ArcGIS software, to test if there is a relation between the *Ksat* value and its location in the catchment. If there is a relation a semivariogram can be fitted to obtain the spatial correlation structure. In case there is no relation found, values for *Ksat* will be randomly generated in PCRaster based on the class average and standard deviation.
In addition, variances of the coupled measurements were evaluated. If the variance between couples is significantly different from that within couples, heterogeneity is present and an

upscaling method can be applied. If the variances are judged to be equal, *Ksat* values will be assigned with equal weights to cells in the classes.

4.3.3 Infiltration: B

The B parameter is a measure of the suction the soil exerts on the available water. It is determined from the *G* parameter and the soil moisture conditions. For this research, the equipment nor the time is available to conduct measurements to determine the soil moisture conditions. Other methods like the BEACH model (Sheikh et al, 2009) require detailed information about the climate and soil conditions that is also not available. Literature exist on values for *G* and the saturated moisture content for the silt loam soil class. However, these values are usually given as a range of numbers, depending on soil conditions, which increases the uncertainty. These problems lead to the choice for an empirical approach where the B parameter will be extracted from the infiltration curve. This method has been applied by Simons and Voortman (2009). The infiltration curve of figure 4.3, derived from the measured infiltration rates, was plotted against the Smith and Parlange curve. The only unknown in the Smith and Parlange equation is the *B* parameter. A value for *B* was inserted and varied until the Smith and Parlange curve matches the infiltration curve. This procedure was carried out for all the measurements resulting in 150 values for *B*. Eventually the *B* values were plotted against their corresponding *Ksat* value to find a (linear) relation between the two parameters resulting in an equation that describes the average of *B* as a function of *Ksat*.
This empirical approach will be compared to the method of deriving *B* from *G*. In this approach *B* will be divided by literature values for *G* (Hantush and Kalin, 2005) to obtain the saturation deficit. If these values fall outside the range of 0.01 (the residual saturation of a silt loam soil) to 0.501 (the porosity and thus maximum saturated of a silt loam soil), they are unrealistic (Rawls et al, 1982). This would indicate that literature values for *G* are not representative for the soils found in the study area. If so, the empirical approach is preferred. The error in *B* is equal to the change in *B* when the error in *Ksat* is added to the Smith and Parlange curve. This is checked for ten randomly chosen measurements to find an average value for the error. If it appears to be large (>5%) it is subtracted from the standard error. The standard error in B is given by the following equation:

$$se_{\hat{B}} = \sqrt{s_B{}^2 (1 + \frac{1}{n} + \frac{(Ks_c - \overline{Ks})^2}{\sum (Ks_i - \overline{Ks})^2}}$$

where $se_{\hat{B}}$ = standard error of the predicted B value, $s_B{}^2$ = the variance of the B values, n = the number of measurements, Ks_c = the saturated hydraulic conductivity of the current grid cell, $\overline{Ks}$ = the average saturated hydraulic conductivity and Ks_i = the observed saturated hydraulic conductivity of a certain measurement.
Eventually, values for *B* undergo another transformation concerned with the implementation of the volumetric rock content. The rock content was estimated in the field as the volume of rock per volume of soil sample at each measurement location. Values were sorted per class and then averaged resulting in one value for *ROC* per class.

4.3.4 Depression storage

The microtopography that is of interest for the depression storage is not visible on the DEM. Richards (2005) invented a device that measures the microscale topography and the slope onsite; the roughness clinometer. Figure 4.4 explains the workings of the device. Rods are lowered onto the ground surface making the microscale topography visible relative to a reference level. These displacements together with the slope give the ideal depression

storage. A correction has to be applied because water will flow over the hills (as shown in figure 4.4), resulting in the effective depression storage. Displacements and slope are measured in the field at every measurement location resulting in 150 depression storage measurements.
Calculation of the effective depression storage was performed using the ROUGH4 software package (Richards, 2005), specially developed for the processing of clinometer data. To serve as input for the model, values for the depression storage were plotted against the corresponding slope to find a (linear) relation between the two. Because the slope is provided by the DEM, the model generated a value for *Dst* for every cell according to the relation that is found.
The standard error in *Dst* was computed according to the equation above for the standard error in *B*. Initially, *Dst* is set to zero all over the catchment.

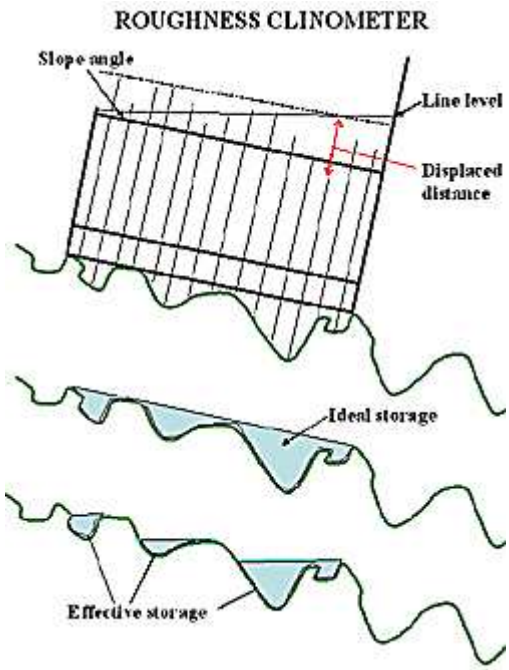

Figure 4.4 Roughness clinometer.

4.3.5 Routing

The most important element of the routing, the DEM, is provided by the US Geological Survey. The DEM includes all large scale elevation differences but neglects some of the smaller, more subtle variations in height, for example the elevated rim next to the sinkhole (visible in figure 4.2). Also, because the DEM is from 1983 the rise in elevation at the former landfill site is not included. The differences this causes in, for example, the flood volume calculation will be estimated rather than adapting the DEM. Variations to the DEM witnessed in the field, like a pipe discharging water to outside the catchment, or the presence or absence of channels, are accounted for. This results in a local drain direction network generated in PCRaster (appendix 2).
Water is routed downstream as sheet flow or as channel flow. For sheet flow, the channel width is equal to the size of the cell. For channel flow, values for channel width are estimated in the field. However, these values are not directly used in the model, because the acquired data is insufficient in number and channel width varies over the length of the channel. Instead, *Bw* was made a function of the number of cells discharging into a particular channel cell. Widths at the origin and outflow point of a channel were fixed. Going downstream from the origin, cells gradually become wider as more cells discharge into that part of the channel. Classification is made based on field estimates and aerial photographs. This way, channels with few cells discharging into them are simulated as narrow and with a large number of cells simulated as wide (appendix 3). The value of the slope angle of the channel is set to 90º.
Values for Manning's n were taken from the literature (Chow, 1959) and are given in table 5.1. These values might be adapted to the definitive class distinction for actual model input. The assumption was made that the floodplain, swamps and urban areas were saturated. Any water that is routed over these areas cannot infiltrate and will be routed downstream without the loss of water.

Table 4.2 The Manning's n values for different land use classes.

Land use	Manning's n
Forest	0.4
Corn	0.15
Beans	0.06
Grassland	0.15
Lawn	0.41
Swamp	0.02
Urban	0.011
Roads	0.011

4.4 Seasonal variability of parameters

To assess the model's sensitivity to a change in one of the parameters, a sensitivity analysis is conducted. This was done is the framework of the parameters variability to seasonal influences. A shift in weather conditions causes values of certain parameters to change. Parameters that were included in the sensitivity analysis were: *Ksat*, *ICmax*, *COV*, *Dst*, *B* and *n*.

The maximum interception store and coverage shift from a high value to a low value from summer to winter because the leaf area index decreases. They were decreased by 20% during winter.

Manning's n becomes higher in the winter season because the roughness of the soil surface increases meaning the ground becomes more brittle. The *n* parameter was increased by 20% during winter.

Seasonal variation within *Ksat* was neglected, assuming no modification of the soil occurs from summer to winter. Depression storage capacity depends solely on the slope. Though these parameters are not affected by seasonal changes, they are still included in the sensitivity analysis, because they are prominent in the model. Both *Ksat* and *Dst* were increased by 20%.

The saturation deficit parameter is dependent on local soil moisture conditions. Values for *B* are either derived empirically or calculated from literature values for *G* and soil moisture conditions. Empirically derived values will be increased with 20%. If the model appears to be sensitive to *B*, sensitivity to the *G* parameter and the initial moisture content will also be assessed. In this case, the initial moisture content will be varied between 0.01, simulating a very dry soil, to 0.501, simulating a saturated soil. The *G* parameter was increased by 20% on top of its literature derived value of 1.05 m (Hantush and Kalin, 2005).

To correctly assess the model's sensitivity to a change in one of the parameters, it was run without random functions. Removing the random component guaranteed that, during a run, the only thing that can cause a change in the output is the parameter that is changed. The analysis criteria were cumulative runoff, peak runoff and time to peak. Cumulative runoff is the most important criterion because it is the main point of interest in this research.

The scenario of January 2010 with saturated floodplain, swamp and urban areas were simulated for this analysis because it has one distinct peak in runoff simplifies the comparison between different parameters.

4.5 Monte Carlo simulation

The random component in the generation of the *Ksat*, *Dst* and *B* parameter values through their normal distribution causes the model output to be slightly different after every run. This variation represents the uncertainty in the model output due to uncertainties in the

model parameter values. Running the model 200 times, each time plotting the cumulative runoff curve, gives the band of uncertainty. This method of generating 200 realizations from repeated random sampling is called Monte Carlo simulation. Plotting a cumulative frequency distribution of the 200 cumulative runoff values gives the possibility to calculate the median, mean and quartiles of the outcome.
The Monte Carlo simulation was run the model with the assumption that in the floodplain, swamps and urban areas no infiltration takes place because the soil is saturated by groundwater. A scenario where these areas are not saturated was also simulated. This will give insight in the portions of runoff being saturated overland flow and Hortonian overland flow. Whether another Monte Carlo simulation will be applied to this *unsaturated* scenario depends on the model's uncertainty. If statistics show that the band of uncertainty is very small for the *saturated* scenario, Monte Carlo simulation was not applied to the *unsaturated* scenario.
The PCRaster model script is provided in appendix 12.

5 Results

5.1 Precipitation timeseries

Model runs for the three scenarios discussed in chapter *4.1.1* resulted in small differences in model output. The hydrographs of the three scenarios are similar. The *normal* and *uniform* scenarios produce respectively the highest and lowest cumulative runoff but the difference is only 4.7%. Because the difference in total runoff volume is small and the hydrographs are similar, the *normal* scenario is chosen for the event modelling. It is also the scenario that closely resembles an actual rainfall event. Preliminary rainfall intensity data from a regional climate station at Syracuse Hancock Airport confirm this.
The assumption that snow will melt linearly over the first twelve hours of a day is justified because the effect of different rainfall scenarios appears to be small. This linear melting is not the case in a real life situation but because the different rainfall scenarios have proved to have little effect on the model output, this approach will suffice.
Adding rain and snowmelt resulted in the timeseries that are used in the event modelling, shown in figure 5.1.

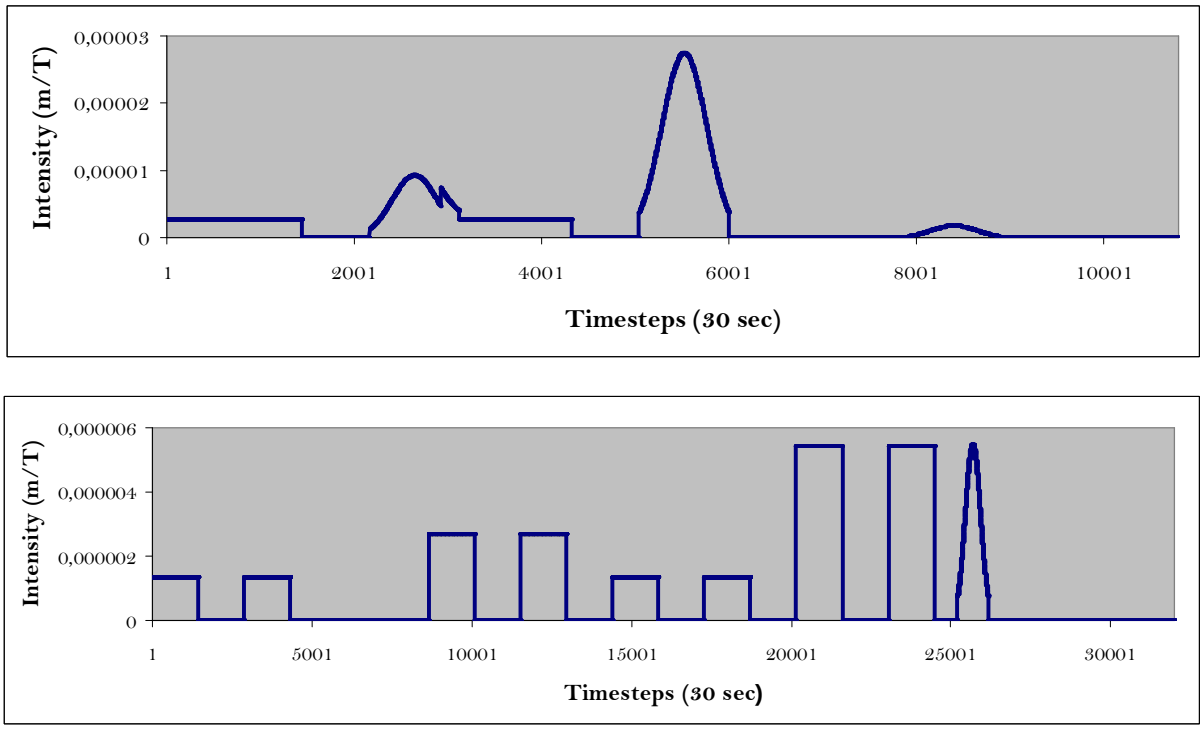

Figure 5.1 Timeseries of precipitation events of January (top) and March (bottom) 2010.

The start of the flood was chosen to be the date the lake starts to rise. The start of the precipitation time series that causes the particular flood was chosen to be one day prior to the start of the flood. Tests with the model running the event of 1994 showed that the time to peak of runoff, the time required for the majority of runoff to reach the sinkhole, is approximately one day. This implies that the majority of any precipitation coming from one day before the start of the rise of the lake cannot contribute to the flood as surface water runoff. The end of the timeseries was chosen to be the date the lake is at its highest level; any runoff arriving later does no longer contribute to the rise of the lake. Consequently, for the events of January and March, the starting dates of the timeseries were January 24th and March 5th, respectively, and the ending dates were January 27th and March 15th, respectively.

5.2 Parameters input

5.2.1 Interception

A total of 150 coverage measurements are conducted. Classifying the data and averaging the values per class yields the values displayed in table 5.1 that are used as input for the model. Values for *roads*, *landfill* and *swamp* were set to a small value.

Table 5.1 The coverage values for different land use classes.

Class	COV (-)
Forest	0.698
Cropland	0.140
Grassland	0.900
Golf/ Lawn	0.900
Swamp	0.0001
Roads	0.0001
Landfill	0.0001

Table 5.2 shows the resulting values for *ICmax* for the different classes, extracted from Breuer et al (2003). The value for *cropland* is averaged from the *corn* and *beans* land use classes. Values for *roads* and *landfill* were set to a small value.

Table 5.2 The maximum interception store values for different land use classes.

Class	ICmax (m)
Forest	0.0011
Cropland	0.00245
Grassland	0.0017
Golf/ Lawn	0.0023
Swamp	0.0001
Roads	0.000001
Landfill	0.000001

5.2.2 Infiltration: Ksat

From the total of 150 conducted double-ring infiltrometer measurements, 146 were used in the further analysis of data. They are tabulated in appendix 4. The other four were discarded from further analysis because the resulting values were zero, implying the soil is saturated. This must be addressed to incorrectly deploying the infiltrometer, because measurements at similar and nearby locations gave normal values. The locations of all the measurements are displayed in appendix 5.
The H0 hypothesis that the data fits a normal distribution was rejected at a significance level of 0.05 using the Kolmogorov-Smirnov test (appendix 6). After log transformation this is still the case for the whole dataset. Performing the same test, but now for each class separately with log transformed values, results in all classes being normally distributed at the 5% significance level. Because values for each parameter are ordered per class and used as input as such, the fact that the data are normal in each class is sufficient.
Analysis of variance tests of the transformed *Ksat* data were performed and showed that the distinction based on land use and hydrologic group is justified. Table 5.3 shows that the F value is larger than the critical F value.

Table 5.3 Overview of the average and variance for different land use classes and the results of the analysis of variance test.

Class	n	Sum	Average	Variance
Forest AB	34	42.2312	1.242092729	1.254861
Cropland BCD	36	-8.8658	-0.246216106	3.350795
Grassland BC	24	12.8895	0.537061965	2.196959
Golf B	14	19.6871	1.406224996	1.348759
Forest C	10	17.792	1.779200272	1.585336
Forest D	6	9.20631	1.534384697	1.288392
Lawn BCD	22	31.2156	1.418889624	1.318931

ANOVA

Source of variation	Sum of sq	d.f.	Avg sq	F	P-value	Critical F
Between groups	73.7339	6	12.2889	6.207	8.54E-06	2.164409
Within groups	275.159	140	1.97956			
Total	348.893	146				

Equality of variances and means was tested with the F-test and t-test. Results were tabulated in appendix 7. The outcome is that various classes can be merged together. However, only the *Golf B* and *Lawn BCD* classes and all the *Forest* classes were merged so that only five classes remain: *Forest*, *Cropland*, *Grassland*, *Golf/Lawn* and *Urban*. Hydrologic group affixes were eliminated because it is no longer a criterion. This means that found values for *Ksat* in this research do not coincide with the classification of the USGS soil survey. Merging of the *Forest* class with the *Golf/Lawn* class was also statistically justified but not desirable because they differ too much in land use, coverage, depression storage and slope.
The spatial correlation of *Ksat* was examined by constructing variograms of all the classes. The variogram of the class with the most measurements is depicted in figure 5.2.

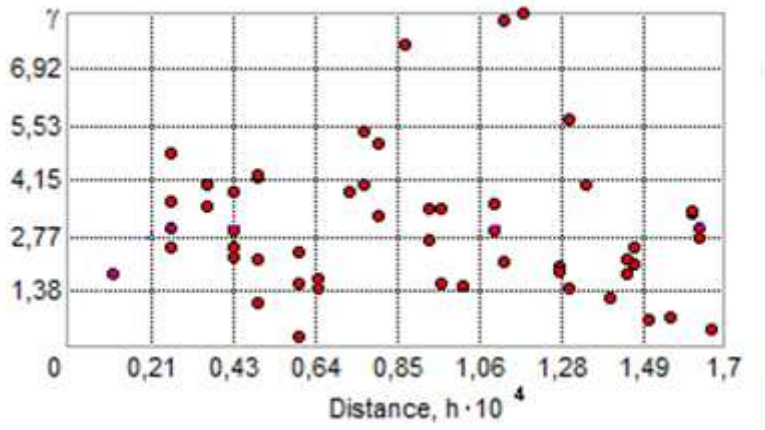

Figure 5.2 Variogram of *Ksat* values in the *cropland* class. Point in the variogram are too scattered to fit a semivariogram.

No semivariogram can be fitted through the data which means there is no spatial correlation between the *Ksat* values. Consequently, values for the log transformed *Ksat* will be randomly generated for each cell according to the normal distribution of its class. The definitive classes and their averages and standard deviations are given in table 5.4.

Table 5.4 The definitive classes and their average and standard deviation.

Class	n	Average	Standard deviation
Forest	50	1.317122	1.62854
Cropland	36	-0.24622	1.830518
Grassland	24	0.537062	1.482214
Golf/Lawn	36	1.531487	1.175806
Urban	0	-	-

Scale dependency of *Ksat* was examined by comparing the variances between couples to the variances within couples. The results are presented in table 5.5. Differences in variances are small. Only in the *Golf/Lawn* class the variance between couples is smaller than the variance within couples. From these results we assumed no scale dependency of *Ksat*.

Table 5.5 Variances between couples against variances within couples for the different classes.

Class	Variance between	Variance within
Forest	0.884834	0.715561
Cropland	1.969702	1.771837
Grassland	1.638876	1.206232
Golf/Lawn	0.818357	1.144213
Urban	-	-

The standard error of *Ksat*, calculated from ten randomly selected measurements, is 1.808% (appendix 8). This number is small enough for the error to be neglected.

5.2.3 Infiltration: B

Plotting all the empirically derived log transformed *B* values against their corresponding log transformed *Ksat* values gives a relation between the two parameters, plotted in figure 5.3. Shown in the figure as well as in the R^2 value is that the relation between *Ksat* and *B* is linear and justified. The equation belonging to this relation, representing the average of *ln B* as a function of *Ksat* is:
*ln(B) = 0.991 * ln(Ksat) - 1.7932.*
The standard error in *B* comes from the equation in paragraph *4.3.3*. Together with the average this is the input for the model. For every cell, a value for *B* is generated from the normal distribution per class of *Ksat* and the standard error of *B* itself.

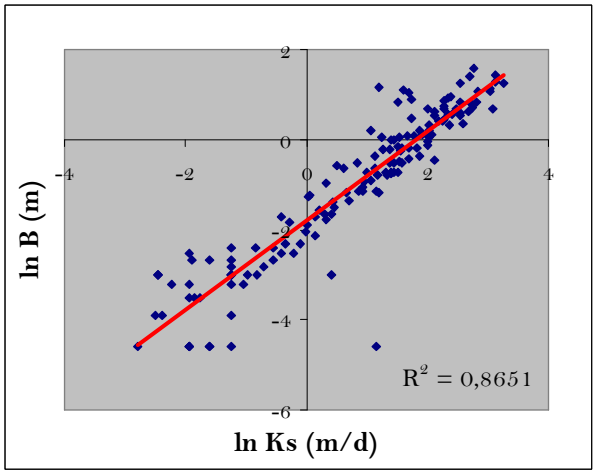

Figure 5.3 Plot of *ln B* vs *ln Ksat*

Empirically derived values for *B* were divided by *G* taken from Hantush and Kalin (2005). From this calculation follows that 77 of 146 measurements fall outside the acceptable saturation deficit range of 0.01 - 0.501. The corresponding average saturation deficit is 0.899. These results support the use of empirical data above literature derived data for this study.
Values for *ROC* are estimated in the field and averaged per class. They are given in table 5.6.

Table 5.6 The volumetric rock content values for the different land use classes.

Class	ROC (-)
Forest	0.0444
Cropland	0.0614
Grassland	0.075
Golf/ Lawn	0.0001
Swamp	0.0001
Roads	0.0001
Landfill	0.0001

5.2.4 Depression storage

Depression storage values were generated in PCRaster from their relation to the slope in the DEM. Plotting the effective depression storage values against the corresponding slopes gives the following linear relations between the two parameters, for each class:

Forest: $ln\ Dst = -0.1276 * x - 5.6483$
Cropland: $ln\ Dst = -0.2935 * x - 4.9646$
Grassland: $ln\ Dst = -0.256 * x - 5.1511$
Golf/Lawn: $ln\ Dst = -0.3067 * x - 6.0694$

where x = slope (%). Depression storage of the *Urban* class is assumed to be zero. Graphs of the relations between *Dst* and x are provided in appendix 9.

5.3 Model output

5.3.1 Water fluxes

Figure 5.4 shows the cumulative fluxes of water during the events of January and March 2010, respectively. The graphs for the two events are similar in the way that the fluxes have the same behaviour. Vegetation intercepts a portion of the precipitation in the beginning, but quickly the maximum interception store is filled and no more water is added. Neglecting evaporation means that once the interception store is filled, it does not empty and no more water can be added for the rest of the event. Microscale depressions capture a small portion of the water that reaches the ground and flows downstream. During peaks in precipitation the depression storage contains the most water. The total precipitation curve is followed closely by the infiltration curve. The majority of the precipitation, after it reaches the ground, infiltrates and will no longer be available for other processes. Therefore, the portion of the total volume of precipitation that becomes runoff is small. Only after the largest precipitation peaks a small peak in runoff is visible. The rest of the event, volumes of generated runoff a very small and therefore not visible in this graph. In between precipitation peaks, fluxes of water are nearly zero because infiltration immediately captures all the incoming direct precipitation. Only small volumes of runoff are generated by the water that is left after infiltration.

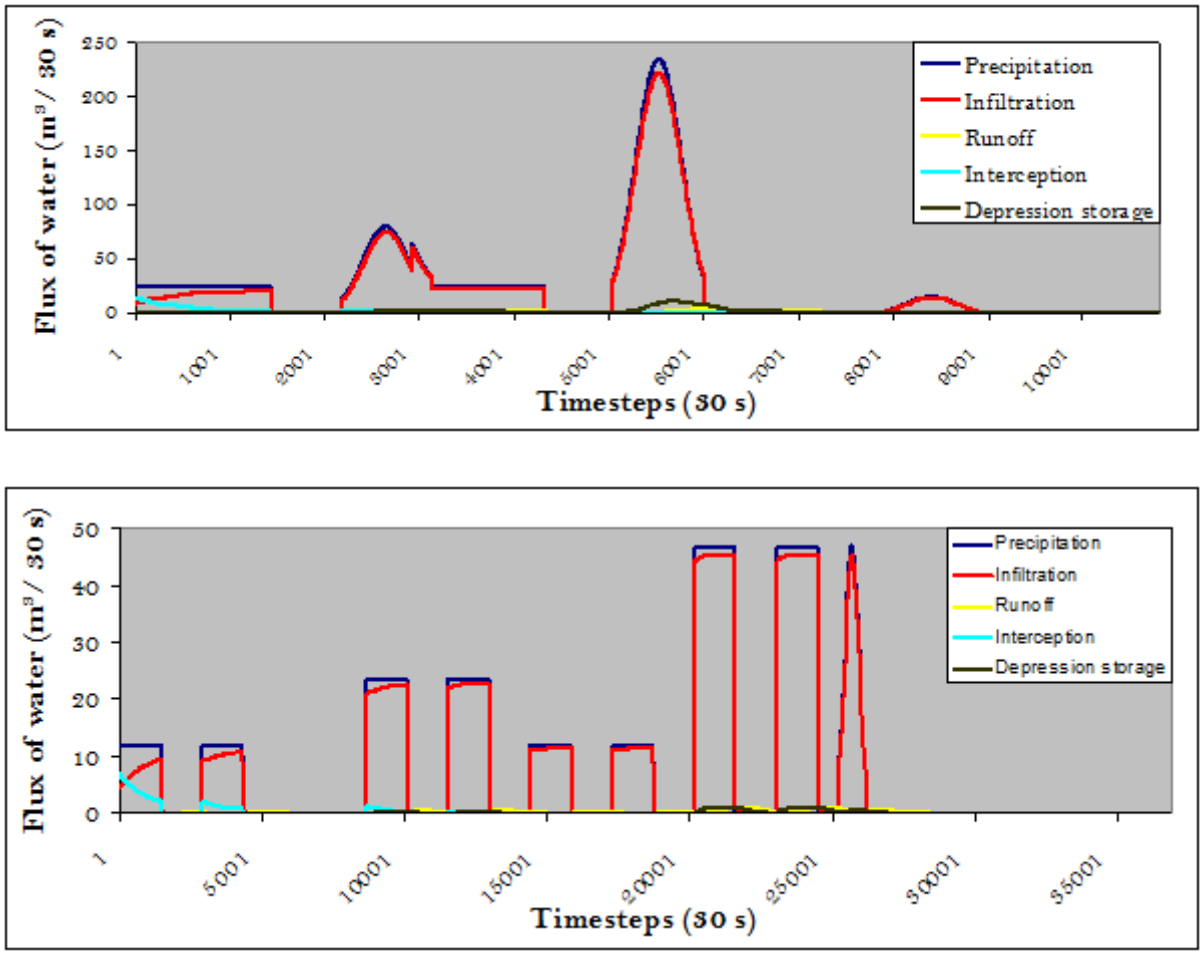

Figure 5.4 Water fluxes of the model processes for January (top) and March (bottom).

5.3.2 Flood volumes

Table 5.7 shows an overview of the lake level data and the flood water volumes calculated using PCRaster. Adaptations to the DEM to improve the volume calculations are included in these calculations.

Table 5.7 Lake level heights and corresponding flood volumes resulting in the added flood volumes during the rise of the lake for both events.

Event	Lake level 1	Flood vol 1	Lake level 2	Flood vol 2	Added flood vol
January 2010	198.7 m	12200 m^3	202.13 m	158611 m^3	146411 m^3
March 2010	198.8 m	14350 m^3	203.6 m	252985 m^3	238635 m^3

Lake level 1 is the lake level at the start of the event, *Lake level 2* the level when the lake reaches its highest point. *Flood volume 1* and *2* are the flood volumes belonging to those lake levels. Subtracting *Flood vol 2* from *Flood vol 1* gives the added volume of water during the rise of the lake. This volume of water can be added by direct precipitation, surface water runoff or other quickflow or groundwater components.

5.3.3 Runoff contributions

Cumulative frequency distributions of the modelled cumulative runoff via Monte Carlo simulation are given in appendix 10 for both events. Table 5.8 shows the statistics of the

cumulative runoff and the contribution of runoff to the flooding events under *saturated* and *unsaturated* conditions. The small difference between the 10th and 90th percentiles of the *saturated* cumulative runoff volumes shows that the band of uncertainty of the model output is very small. This is depicted in appendix 11. Therefore, another Monte Carlo simulation for the *unsaturated* scenario is not required.
The cumulative runoff volumes from a single model run for the *unsaturated* scenario are approximately 2% of the *saturated* cumulative runoff volumes. Differences in cumulative runoff between the two events are explained by the total precipitation volume. Table 5.9 shows the runoff coefficient for both events.

Table 5.8 Overview of the cumulative runoff volumes and corresponding runoff contributions for both events for the *saturated* and *unsaturated* scenarios.

Cumulative runoff volume (m³)					Runoff contribution to flood (%)			
Event	**n**	**10th perc**	**median**	**90th perc**	**Flood vol (m³)**	**10th perc**	**median**	**90th perc**
saturated January	200	7394	7420	7443	146411	5.05	5.07	5.08
saturated March	200	9475	9501	9533	238635	3.97	3.98	3.99
unsaturated January	1	-	158.4	-	146411	-	0.107	-
unsaturated March	1	-	298.5	-	238635	-	0.12	-

Table 5.9 Precipitation volumes of both events and scenarios with calculated runoff coefficients.

Event	Precipitation vol (m³)	Mean cumulative runoff vol (m³)	Runoff coefficient
saturated January	255386	7420	0.0291
saturated March	294808	9501	0.0322
unsaturated January	255386	158.4	0.00062
unsaturated March	294808	298.5	0.00101

5.3.4 Seasonal variability

The effects of a shift in season from summer to winter on the modelled parameters are shown in table 5.10.

Table 5.10 Overview of the changes in parameters with corresponding results on the different analysis criteria.

Scenario	Cum runoff (m³)	Difference (%)	Peak runoff (m³)	Time to peak (T)
normal	7363.4	-	4.5946	6003
-20% *COV*	7377.2	+0.187	4.5983	6003
-20% *ICmax*	7377.2	+0.187	4.5985	6003
+20% *n*	7209.8	-2.086	4.2467	6078
+20% *B*	7363	-0.006	4.5945	6003
+20% *Ksat*	7362.1	-0.0002	4.5944	6003
+20% *Dst*	7296.7	-0.905	4.5789	6004

Resulting variations in cumulative runoff are significant for the vegetation parameters and depression storage, but especially for Manning's n. A change in saturated hydraulic conductivity or the empirically derived saturation deficit parameter has a minimal effect. The lack of the model's sensitivity to the B parameter implies that a further sensitivity analysis of the different parameters comprising B is not required.
Variations in peak runoff values are insignificant with the exception of Manning's n which produces a lower peak. In addition, the time to peak occurs later than in the other scenarios.

6 Discussion

To assure that the model that is used simulates a rainfall-runoff event the best way possible, it is usually calibrated. This means that model results will be compared and adapted to field data. In this study, calibration of the model was not possible because surface runoff measurements from previous studies do not exist, so there is no data to compare the model's results to. Furthermore, the hypothesis of Proett (1978) that groundwater contributes to the flooding and that it most likely interacts with surface runoff implies that there is uncertainty in the composition of the quickflow component. Because of this reason Simons and Voortman (2009) were not able to calibrate the model either, but they did found model results to be consistent with field data. A large dataset of acquired field data for this research contributes to the accuracy of the model. A coarse accuracy test was performed by, one by one neglecting the different model components, and comparing the cumulative runoff volumes that the model produced. If the infiltration term was neglected, almost all of the incoming precipitation ended up as runoff whereas neglecting the interception term had only little effect on the cumulative runoff volume. Therefore, despite the lack of calibration, the assumption was made that the model behaves correctly and sufficiently accurately for this study.

The initial moisture content of the soil, though not measured or varied during this research due to constraints in time and equipment, is an important parameter because it determines the ability of the soil to attract water and therefore it influences the infiltration rate. This parameter is included in the saturation deficit parameter which is derived empirically in this research. These values are derived under saturated conditions because the soil was wetted prior to any measurement. These conditions are assumed to be true at the start of the modelled events. Prior to both of the events large volumes of snow have melted suggesting that the moisture content of the soil has reached a high value close to, or at, the point of saturation. The other method of deriving the B parameter from literature based values for G yielded 77 out of 146 unrealistic values for the moisture deficit. This shows that empirically found values are preferred in this research.

The polje's basin, swamp areas and the urban areas are assumed to be saturated and therefore they are mapped as impermeable. Water entering such a cell will be immediately routed downstream without any loss of water. The surface areas of these land uses is of major influence to the cumulative runoff volume that is generated by the model. Results show that 98% of the generated runoff volumes comes from impermeable areas. This implies that a change in the surface area of the impermeable regions has a major effect on the generated runoff volumes. The extent of the polje's basin is derived from the DEM and is assumed to be correct. However, the area of the swamps is subject to change. The area is currently mapped as it is during a flooding event, based on aerial photographs. The extent of the swamp areas is therefore large in comparison to more drier periods in a year. Transducer data shows that the lake levels prior to the events modelled in this study are very low. Consequently, the swamp areas as they are currently mapped are an overestimate and so are the cumulative runoff volumes. However, the urban land use class includes roads and the former landfill but does not include houses and driveways. This will provide an extra impermeable surface, increasing generated runoff volumes. The current cumulative runoff volumes are calculated from the best estimates possible concerning the impermeable areas. Quantifying the contributions of increased or decreased impermeable surfaces on generated runoff volumes requires detailed information about the changes in surface area.

From the water fluxes graph (figure 5.4) is it clear that peaks in precipitation coincide with peaks in infiltration. In fact, the only difference between the two curves is that the

infiltration curve has slightly lower values. Though depression storage and interception capture some of the precipitation, the high saturated hydraulic conductivity values cause infiltration to be the limiting factor in runoff generation. A typical saturated hydraulic conductivity value for a silt loam is 0.45 cm/hour or 0.108 m/day (Leij et al, 1996). Simons and Voortman (2009) found similar values for their silt loam soils approximately 150 km to the west. In this research, the average *Ksat* value from the 146 double-ring infiltrometer measurements is 5.2 m/day. McKay et al (1993) explains that during the installation of measurement devices, smearing or widening of fractures can occur, causing the saturated hydraulic conductivity to vary with three orders of magnitude between different measuring devices. However, the same infiltrometers have been used as in the study of Simons and Voortman (2009), so this significant discrepancy between literature and field values cannot be attributed to incorrect measurement or analysis techniques. The high *Ksat* values have to be attributed to local soil conditions and can be explained by the occurrence of fractures and macropores in the soil.

The sensitivity analysis has proved that changes in the saturated hydraulic conductivity and the saturation deficit parameter, two parameters that are active in the process of infiltration, have very little effect on the cumulative runoff volume. This can be attributed to the fact that the *Ksat* values that have been measured exceed precipitation intensities. *Ksat* input values are one order of magnitude larger than the maximum precipitation intensity for both events. In comparison to average precipitation intensity they are even two orders of magnitude larger. This problem is enlarged by the fact that 98% of the cumulative runoff volume comes from the impermeable areas. In a simulation including impermeable areas, only 2% of the generated runoff volume is Hortonian overland flow i.e. comes from areas where infiltration is active. The other part is saturated overland flow. This implies that variations in the infiltration rate will only have effect on that 2% of generated runoff. Moreover, a 20% increase of infiltration parameters will have little effect on that 2% because the saturated hydraulic conductivity will still exceed the precipitation intensity.
For these reasons, a further sensitivity analysis of the *B* parameter where the initial moisture content will be varied, is not required. Even when the initial moisture content is equal to the saturated moisture content i.e. the moisture deficit is zero, will infiltration rates exceed precipitation intensities. Whereas infiltration parameters have little effect on model output, the other parameters concerned with the sensitivity analysis show significant changes in cumulative runoff volumes. The model is most sensitive to Manning's n and depression storage because they affect runoff generation without interfering with the process of infiltration. The influence of the interception parameters is less because the amounts of water stored in vegetation are relatively small.

The simulation of the runoff production in the Disappearing Lake has shown that surface water runoff only accounts for a 5% of the total flood volume. Differences in cumulative runoff volumes between the two events are explained by the differences in total precipitation volumes. Small uncertainties in flood volume calculation and the extent of impermeable areas do not impede with the fact that other water sources have a bigger share in the flooding of the polje. The volume added by direct precipitation onto the lake must be neglected. The total amount of precipitation over the entire catchment as a layer of water is 2.98 cm and 3.44 cm for January and March respectively. The amount falling directly onto the lake is at least a factor ten smaller due to differences in surface area. The contribution of these few millimetres added to a certain lake level is for that reason neglected. Besides surface runoff, another quickflow component that has not been accounted for could contribute to the flooding. In the streams discharging into the lake, multiple locations were found where water disappears and resurges farther downstream. This phenomenon was not taken into account in the model. However, though not as quick as surface runoff, this runoff

component can contribute to the erratic lake level fluctuations. The volume of the water flux concerned with this component is hard to quantify. Nonetheless, the large infiltration rates result in large volumes of water in the unsaturated zone that could contribute to the flooding as shallow, sometimes resurging, subsurface quickflow.

The relatively small contribution of modelled surface runoff to the flooding events implies that other water sources have a larger share in the flooding. This unknown major source of water could originate from groundwater upwelling. This hypothesis is supported by the fact that floods only occur in late winter and spring, times when the water table is relatively high. Transducer and climate data reveal an interesting process prior to the event of January (figure 4.1). First, a large snowmelt event in combination with small rainfall events causes the water table to rise to about 1-1.5 m above the sinkhole. Approximately 10 days later, the water table still around this elevation, the precipitation events that are modelled in the January event occur and the lake erratically rises. A water table at the elevation of the sinkhole could be a criterion for flooding events to occur. The major part of the flood volume must come from other sources. Tracer studies can be performed to give more insight into the contributions of other quickflow or groundwater components. With the current knowledge, the Disappearing Lake does not appear to be a mainly surface water runoff driven phenomenon. To which extent it is driven by other quickflow or groundwater component remains unknown.

7 Conclusions and recommendations

This study has quantified the contribution of surface water runoff to two flooding events in the Disappearing Lake valley in 2010. Infiltration measurements were conducted on different land uses to obtain values for the saturated hydraulic conductivity. These values served as input for the infiltration model that was used in a rainfall- runoff model to simulate runoff generation in the catchment. After Monte Carlo simulation, average generated runoff volumes were compared to calculated flood volumes to evaluate the contribution of surface runoff to the two flooding events. In addition, the sensitivity of the model output to changes in model parameters was assessed. From this study the following conclusions can be drawn:

- Sensitivity of the model to seasonal variability within parameters is expressed by Manning's n and depression storage. The model is not sensitive to changes in the saturated hydraulic conductivity and the saturation deficit parameter due to high infiltration rates and the fact that almost all of the runoff comes from saturated areas.

- The large measured saturated hydraulic conductivity values that result in small runoff volumes, do not coincide with literature values nor with values measured by Simons and Voortman for a silt loam soil. Though this could well be attributed to local soil conditions, other measurements techniques could be applied in the study area to clarify this discrepancy.

- From the generated volume of runoff, 98% comes from the saturated areas. The remaining portion is Hortonian overland flow. This is explained by the fact that infiltration rates exceed precipitation intensities.

- The contribution of surface runoff the flooding events of January and March 2010, assuming the polje's basin and swamps to be saturated, is respectively 5 and 4%. If the polje's basin and swamps are not saturated, almost all the water infiltrates and less than 1% of the flood is explained by surface runoff.

- The contribution of the surface water runoff component to the flooding of the Disappearing Lake is small and suggests that other sources, for example subsurface quickflow and groundwater upwelling could contribute of the flood. The exact size of these source of water remains unknown.

- The Disappearing Lake does not appear to be a mainly surface water runoff driven phenomenon, whereas other sites along the Onondaga Formation investigated by Simons and Voortman have a larger influence of surface runoff. Research on other sites has to be conducted to make any statements on a possible regional groundwater phenomenon.

- Whereas this study is focused on quantifying the runoff component, investigating subsurface flow and groundwater upwelling is needed to give a clear explanation of the mechanisms behind the flooding of Disappearing Lake. A tracer study can be performed to estimate the contribution of subsurface quickflow and groundwater upwelling to the flooding of the lake.

References

Allenson, S.T. 1955. Stratigraphy and structure of the southern part of the Camillus quadrangle, Onondaga County, New York: Master's thesis, Syracuse University, 105 p.

Baxter, M.A., Graves, C.E., Moore, J.T. 2004. A Climatology of Snow-to-Liquid Ratio for the Contiguous United States, Department of Earth and Atmospheric Sciences, Saint Louis University, St. Louis, Missouri, Vol. 20, p. 729-744.

Bierkens, M.F.P. 1994. Complex confining layers: a stochastic analysis of hydraulic properties at various scales, Netherlands Geographical Studies 184, Utrecht University, 263 p.

Breuer, L. , Eckhardt, E. and Frede, H-G. 2003. Plant parameter values for models in temperate climates, Ecological Modelling 169 (2-3), p. 237-293.

Chow, V. T. 1959. Open-channel hydraulics, Mc-Graw-Hill, New York.

Fairchild, H.L. 1909. Glacial waters in central New York: State Mus. Bull. 127, 59 p.

Hantush, M. M. and Kalin, L. 2005. Uncertainty and sensitivity analysis of runoff and sediment yield in a small agricultural watershed with KINEROS2, Hydrological Sciences Journal, 50: 6, p. 1151-1171.

Krall, D.B. 1966. Fluvioglacial drainage between Skaneateles and Syracuse, New York: Master's thesis, Syracuse University, 158 p.

Leij, F. J., W. J. Alves, M. Th. van Genuchten, and J. R. Williams. 1996. The UNSODA Unsaturated Soil Hydraulic Database; User's Manual, Version 1.0. EPA/600/R-96/095, National Risk Management Laboratory, Office of Research and Development, U.S. Environmental Protection Agency, Cincinnati, OH. 103 p.

McKey, L.D., Cherry, J.A., Gillham, R.W. 1993. Field experiments in a fractured clay till, Water resources research, Vol. 29, No. 4, p. 1149-1162.

Merriam, R.A. 1973. Fog drip from artificial leaves in a fog wind tunnel, Water Resources Research 9, p. 1591-1598.

Mishra, S.K., Tyagi, J.V. and Singh, V.P. 2003. Comparison of infiltration models, Hydrological processes 17, p. 2629-2652.

Morgan, R.P.C., Quinton, J.N., Smith, R.E., Govers, G., Poesen, J.W.A., Auerswald, K., Chisci, G., Torri, D., Styczen, M.E. 1995. The European soil erosion model EUROSEM: a dynamic approach for predicting sediment transport from fields and small catchments, Earth Surface Processes and Landforms 23 (6), p. 527-544.

PCRaster. 2008.PCRaster Manual. http://pcraster.geo.uu.nl/

Peel M.C., Finlayson B.L. and McMahon T.A. 2007. Updated world map of the Koppen-Geiger climate classification, Hydrology and Earth System Sciences 11, p. 1633-1644.

Petrik, M. 1965. Lakes in the Croatian limestone region: Hydrol. fractured rocks, Proc. Dubrovnik Symposium, AIHS-UNESCO, v.2, p. 565-589.

Proett, B.A. 1978. Hydrogeology of Marcellus Disappearing Lake, undergraduate thesis, Syracuse University, 118 p.

Rawls, W.J., Brakensiek, D.L., Sexton, K.E. 1982. Estimation of soil water properties, Transactions of the ASEA 25, p. 1316-1328.

Richards, P.L. 2005. A device for measuring depression storage and slope in the field, SUNY College at Brockport. http://vortex.weather.brockport.edu/~pauljr/dep_dev1.htm

Richards, P.L., Norris, M.D., Lin, B.B. 2008. The hydrologic implications of ecologic succession: depression storage and leaf litter. ESA annual meeting, Milwaukee, Wisconsin.

Sheikh, V., Visser, S., Stroosnijder, L. 2009. A simple model to predict soil moisture: Bridging Event and Continuous Hydological (BEACH) modelling, Environmental Modelling & Software (24) p. 542-556.

Simons, G.W.H. and Voortman, B.R. 2009. Quantifying the contribution of surface runoff to karst-related flooding between Le Roy and Caledonia, Master's thesis, Utrecht University, 81 p.

Smith, R.E. and Parlange, J,-Y. 1978. A parameter-efficient hydrologic infiltration model, Water Resources Research 14(3), p. 533-538.

U.S. Department of Agriculture, Natural Resources Conservation Service. 2009. National Engineering Handbook, Title 210-VI, Part 630, Chapter 7, Hydrologic Soil Groups. Washington, DC.

Wilshusen, J.P. 1976. The phantom: Pennsylvania Geology, v.7, No.3, p.9-11.

Woolhiser, D.A., Smith R.E. and Goodrich, D.C. 1990. KINEROS, a kinematic runoff and erosion model: documentation and user manual.

Yimer, F., Messing, I., Ledin, S., Abdelkadir, A. 2008. Effects of different land use types on infiltration capacity in a catchment in the highlands of Ethiopia, Soil Use and Management, Vol. 24, Iss. 4, p. 344-349.

Zarrielo, P.J. 1999, A Precipitation-Runoff Model for part of the Ninemile Creek Watershed near Camillus, Onondaga County, New York, Water resources investigations report 98-4201, U.S. Geological Survey, 60 p.

Zhou, W. 2006. Drainage and flooding in karst terrains, Environmental Geology 51, p. 963-973.

Appendices

List of appendices

Appendix 1 Digital Elevation Model of the catchment

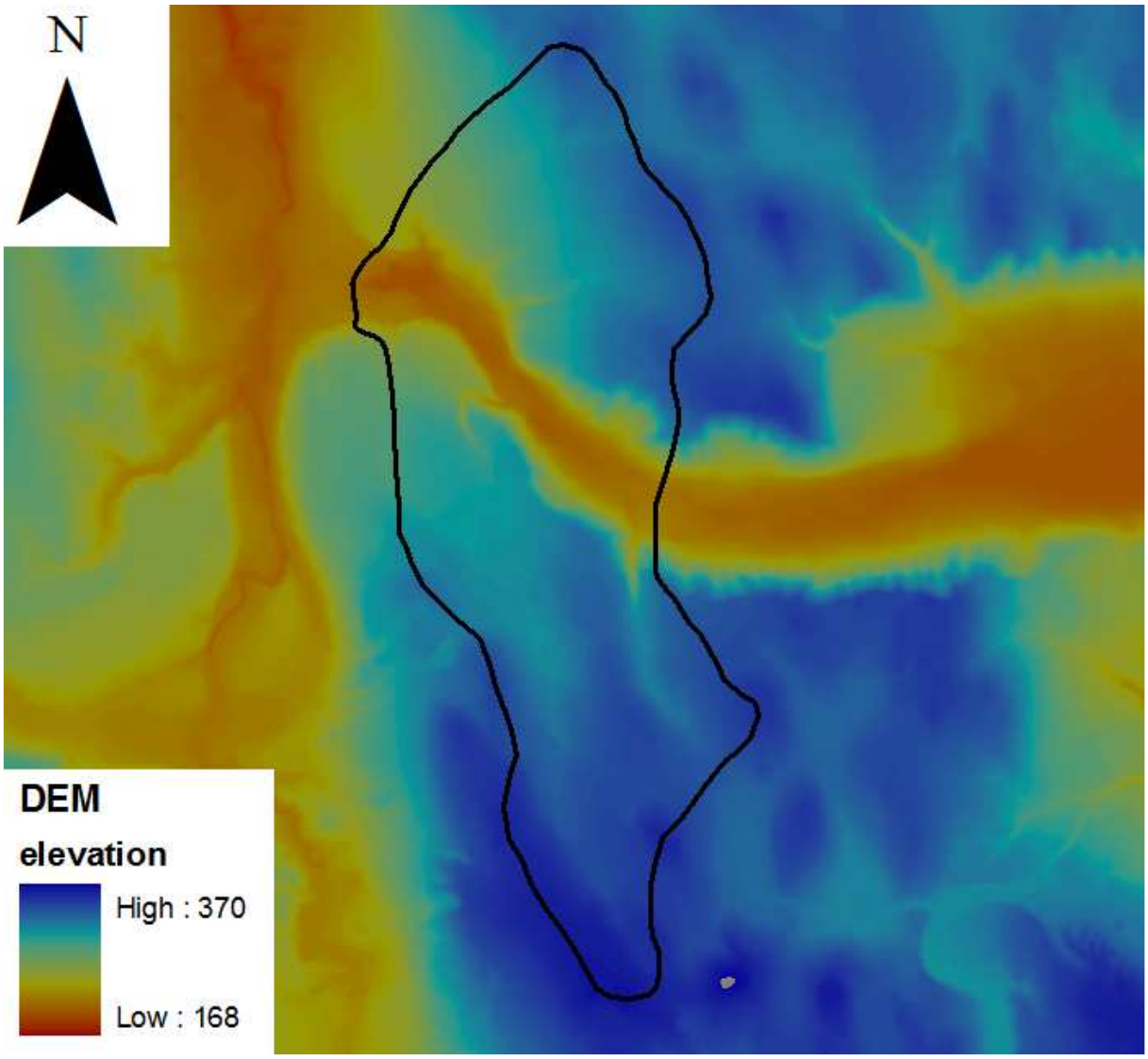

The catchment boundary is shown by the black line. Ninemile Creek is visible west of the catchment. The polje's basin is visible in the north-western part of the catchment. The adjacent west-east trending Cedarvale Meltwater Channel is attached to the basin.

Appendix 2 Local drain direction network

Northern part:

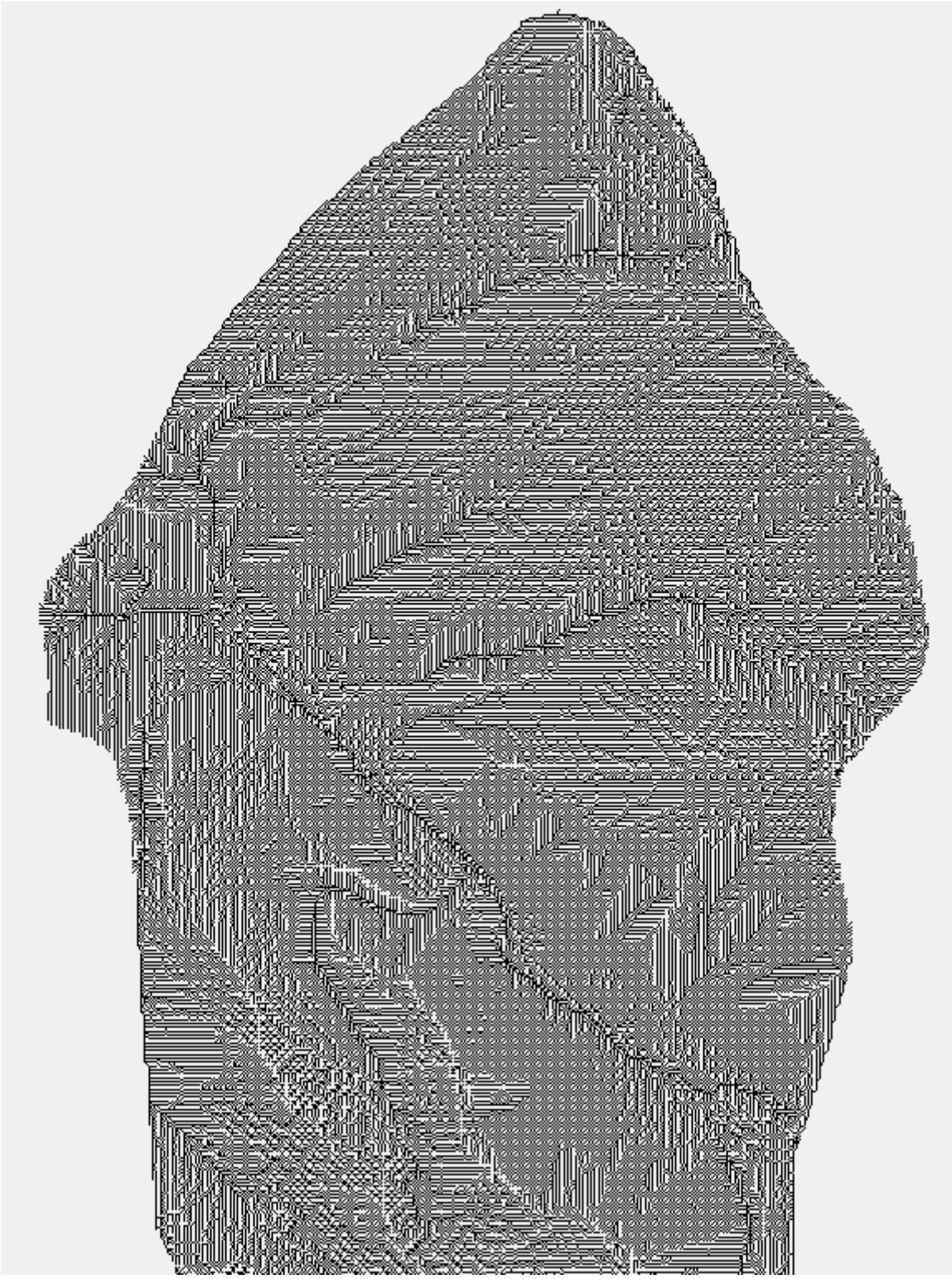

Southern part:

Appendix 3 Channel width of the streams

Values for channel width are in meters. The red colour means no channel is present. In this case water is routed downstream as sheetflow.

.

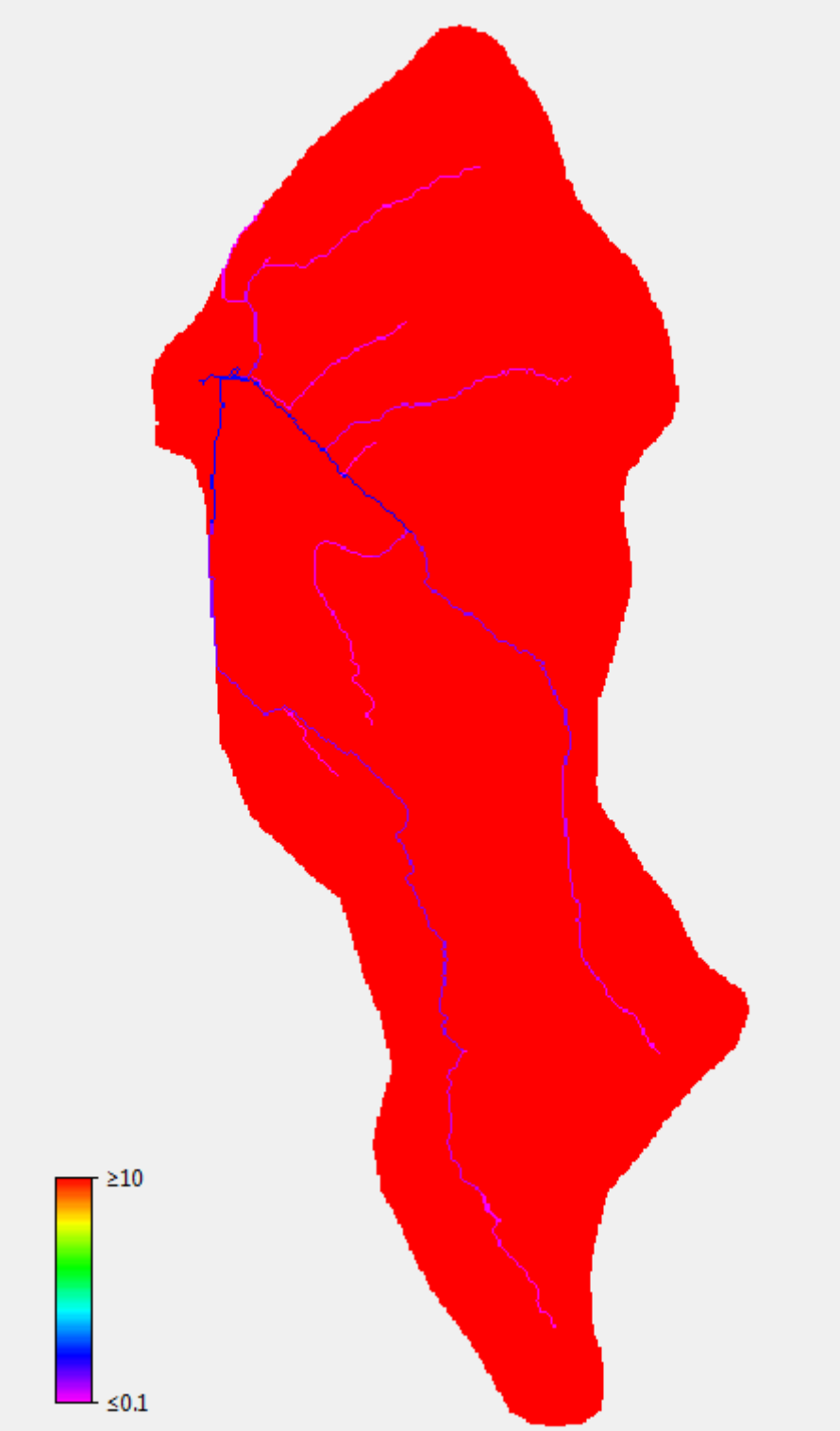

Appendix 4 Overview of all *Ksat, ROC* and *COV* measurements

Measurements are sorted according to the first distinction based on land use classes in combination with hydrologic group. Values for *Ksat* are in cm/min. An 'x' indicates an incorrect measurement.

Forest AB	*Ksat*	*Rock content*	*Coverage*
2A	0,006	0	70
2B	0,1623	0	70
4A	0,278	0	80
4B	0,2164	0	80
10A	0,2817	0	60
10B	0,0971	0	60
11A	0,23	5	80
11B	0,7183	5	80
12A	0,416	5	80
12B	0,0726	5	80
13A	0,886	5	70
13B	0,512	5	70
14A	0,2	0	60
14B	0,344	0	60
15A	0,328	0	70
15B	0,772	0	70
16A	0,244	5	80
16B	0,1643	5	80
20A	0,0526	0	90
20B	0,04	0	90
21A	0,882	30	80
21B	0,38	30	80
22A	0,3771	10	50
22B	0,5183	10	50
23A	0,129	0	70
23B	1,18	0	70
24A	0,39	0	80
24B	0,1873	0	80
25A	0,39	10	60
25B	0,322	10	60
26A	0,1414	0	70
26B	0,0243	0	70
72A	0,75	0	50
72B	0,72	0	50

Forest C	*Ksat*	*Rock content*	*Coverage*
5A	0,8327	5	60
5B	0,3673	5	60
6A	0,336	5	70
6B	0,202	5	70
8A	0,108	0	40
8B	0,08	0	40
9A	0,68	10	90
9B	0,68	10	90
17A	0,3257	20	80

17B	1,4349	20	80
18A	0,1157	5	70
18B	1	5	70
19A	0,24	0	80
19B	0,02	0	80

Forest D	*Ksat*	*Rock content*	*Coverage*
1A	0,67	5	70
1B	0,6789	5	70
3A	0,08	0	40
3B	0,07	0	40
7A	0,574	0	85
7B	0,764	0	85

Grassland	*Ksat*	*Rock content*	*Coverage*
31A	0,316	0	100
31B	0,134	0	100
32A	0,068	0	100
32B	0,02	0	100
33A	0,22	5	100
33B	0,02	5	100
39A	0,106	0	100
39B	0,056	0	100
40A	0,03	2	100
40B	0,0109	2	100
44A	0,026	0	100
44B	0,46	0	100
46A	0,2843	0	100
46B	0,175	0	100
47A	0,2843	0	100
47B	0,074	0	100
49A	0,528	2	100
49B	0,2329	2	100
54A	0,522	0	100
54B	1,5064	0	100
67A	0,377	0	100
67B	1,064	0	100
75A	0,034	0	100
75B	0,58	0	100

Cropland	*Ksat*	*Rock content*	*Coverage*
34A	0,01	0	20
34B	x	x	x
35A	0,2657	10	20
35B	0,104	10	20
36A	0,2926	10	20
36B	0,01	10	20
37A	0,0343	10	20
37B	0,428	10	20
38A	0,0043	10	0
38B	0,01	10	0
41A	0,02	20	30

41B	0,0105	20	30
42A	0,02	0	30
42B	0,04	0	30
43A	x	x	x
43B	0,0064	0	10
45A	0,6531	5	10
45B	0,5336	5	10
48A	0,454	0	10
48B	0,3117	0	10
50A	0,02	15	15
50B	0,0074	15	15
51A	0,5833	10	20
51B	0,006	10	20
52A	0,014	0	20
52B	0,02	0	20
53A	0,01	5	5
53B	x	x	x
55A	0,01	2	5
55B	x	x	x
69A	0,34	5	10
69B	0,014	5	10
70A	0,02	5	20
70B	0,014	5	20
71A	0,176	0	5
71B	0,52	0	5
73A	0,0057	5	0
73B	0,012	5	0
74A	1,04	2	0
74B	1,1	2	0

Golf B	*Ksat*	*Rock content*	*Coverage*
27A	0,256	0	100
27B	1,573	0	100
28A	1,1543	0	100
28B	0,8752	0	100
29A	0,7317	0	100
29B	0,575	0	100
30A	1,57	0	100
30B	0,1109	0	100
66A	0,0495	0	100
66B	0,0943	0	100

Lawn	*Ksat*	*Rock content*	*Coverage*
56A	1,7926	0	100
56B	0,0857	0	100
57A	0,046	0	100
57B	0,182	0	100
58A	1,4343	0	100
58B	0,3157	0	100
59A	0,296	0	100
59B	0,02	0	100
60A	0,886	0	100

60B	0,22223	0	100
61A	0,452	0	100
61B	0,62	0	100
62A	0,216	0	100
62B	0,096	0	100
63A	0,2971	0	100
63B	0,47	0	100
64A	0,0621	0	100
64B	0,2257	0	100
65A	1,0811	0	100
65B	0,926	0	100
68A	0,5543	0	100
68B	0,276	0	100

Appendix 5 Locations of all saturated hydraulic conductivity measurements and land use classes

Measurement locations are shown as black dots. Eventually, all the *Forest* classes were merged and the *Golf* and *Lawn* classes were merged. The *Swamp* class includes the polje's basin.

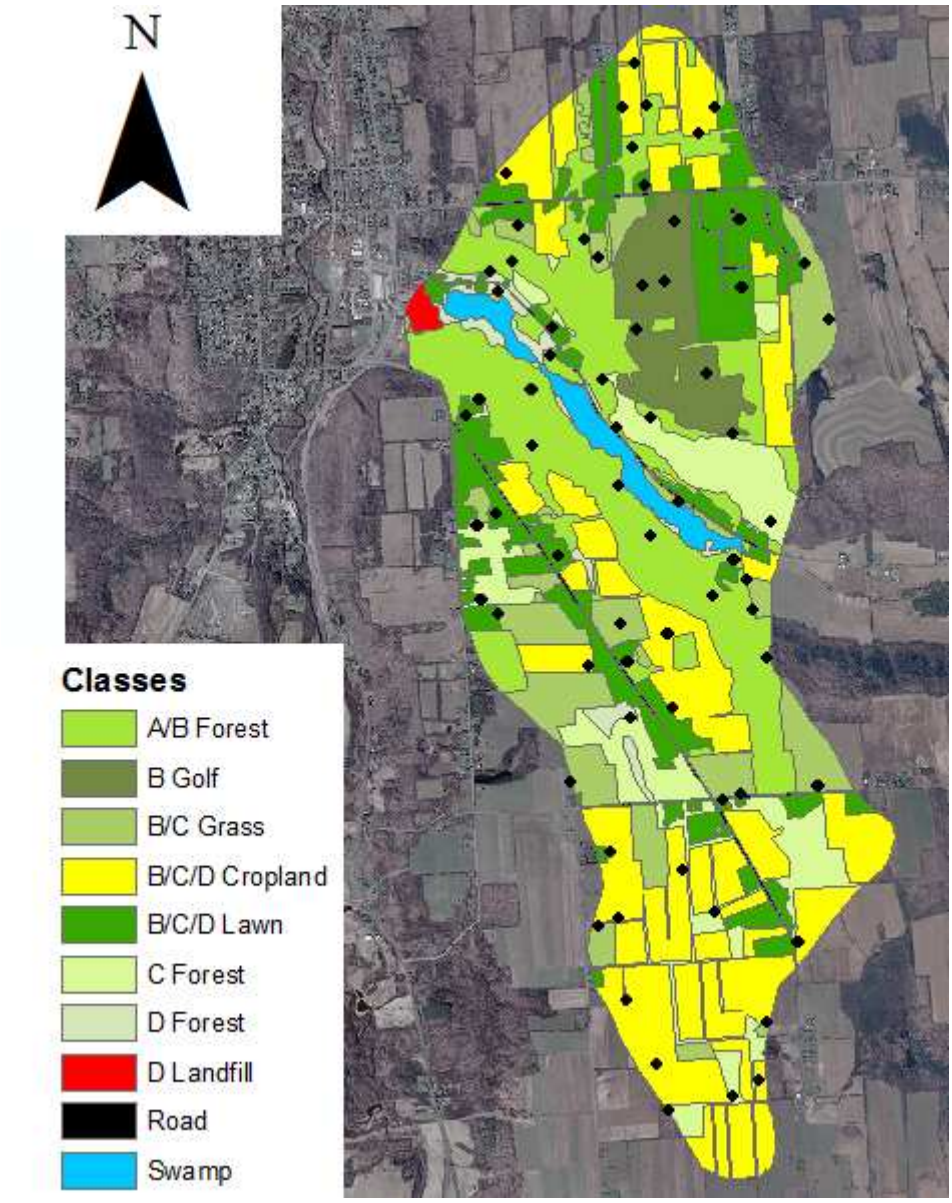

.

Appendix 6 Kolmogorov-Smirnov tests

Visualization of a fitted normal distribution through all 146 untransformed saturated hydraulic conductivity values. The H0 hypothesis that the data fits a normal distribution is rejected for all significance levels. The hypothesis is also rejected using the Anderson-Darling method.

$\mu = 0.3657$

$\sigma = 0.3876$

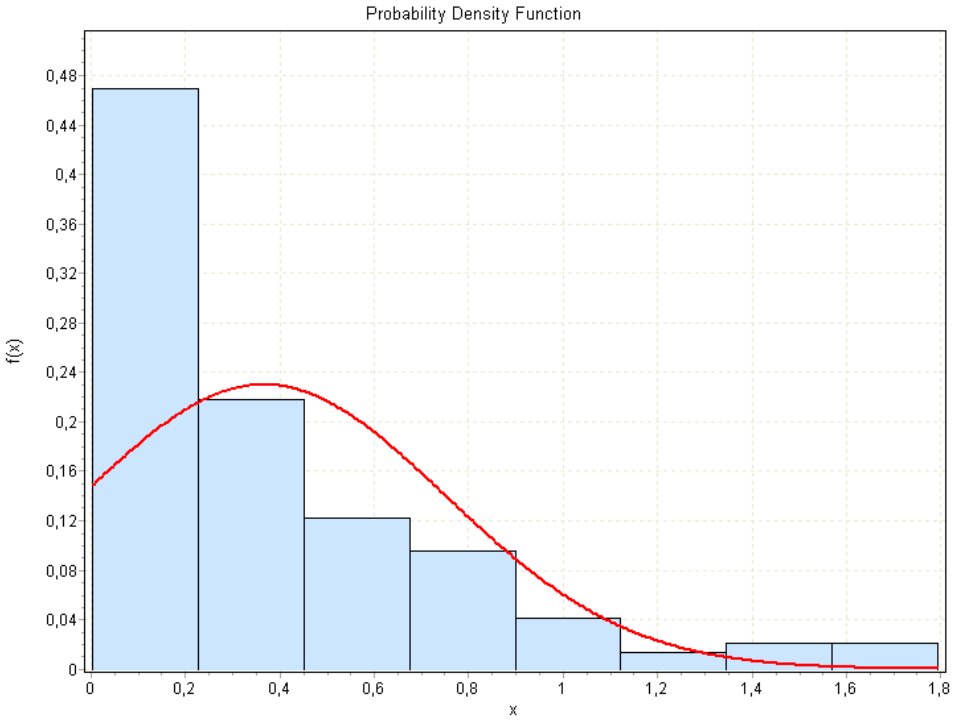

Kolmogorov-Smirnov					
Sample Size Statistic P-Value Rank	146 0,17674 1,8451E-4 39				
α	0,2	0,1	0,05	0,02	0,01
Critical Value	0,0888	0,10122	0,11239	0,12563	0,13482
Reject?	Yes	Yes	Yes	Yes	Yes
Anderson-Darling					
Sample Size Statistic Rank	146 7,0697 35				
α	0,2	0,1	0,05	0,02	0,01
Critical Value	1,3749	1,9286	2,5018	3,2892	3,9074
Reject?	Yes	Yes	Yes	Yes	Yes

Visualization of a fitted normal distribution through all 146 saturated hydraulic conductivity values after *ln transformation*. The H0 hypothesis that the data fits a normal distribution is rejected for all significance levels. Using the Anderson-Darling method the hypothesis is not rejected for the largest significance level, indicating the data is at least more normal that the untransformed data.

μ = -1.8129

σ = 1.5466

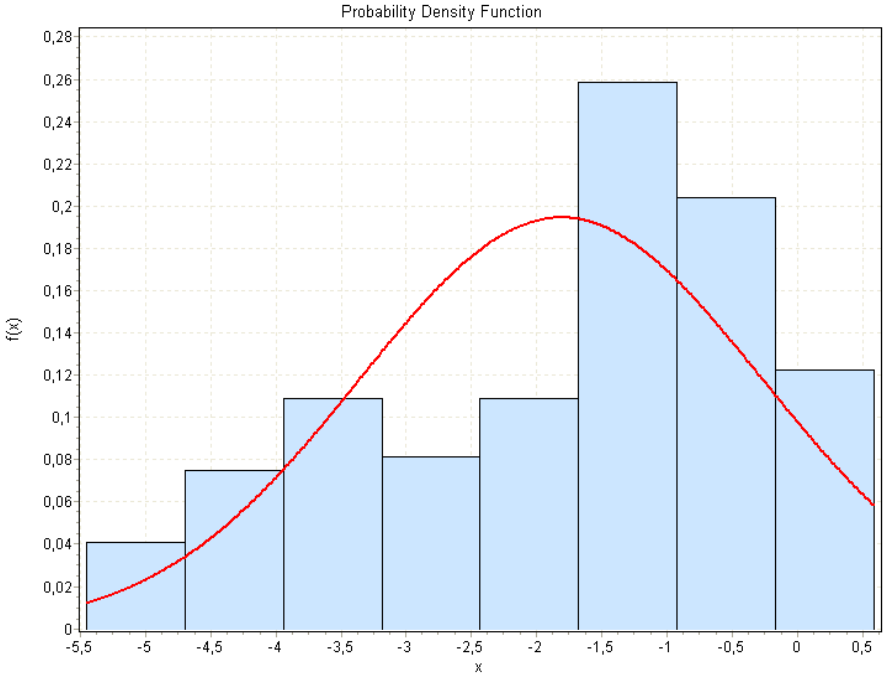

Kolmogorov-Smirnov					
Sample Size Statistic P-Value Rank	146 0,13697 0,00751 18				
α	0,2	0,1	0,05	0,02	0,01
Critical Value	0,0888	0,10122	0,11239	0,12563	0,13482
Reject?	Yes	Yes	Yes	Yes	Yes
Anderson-Darling					
Sample Size Statistic Rank	146 3,533 14				
α	0,2	0,1	0,05	0,02	0,01
Critical Value	1,3749	1,9286	2,5018	3,2892	3,9074
Reject?	Yes	Yes	Yes	Yes	No

The same tests were performed for all the classes with *ln transformed* values. The visualization below is from the *AB Forest class* to give an example. The H0 hypothesis is not rejected meaning the data fits a normal distribution. The same results were obtained for all classes. For the *AB Forest:*

μ = -1.4251

σ = 1.1036

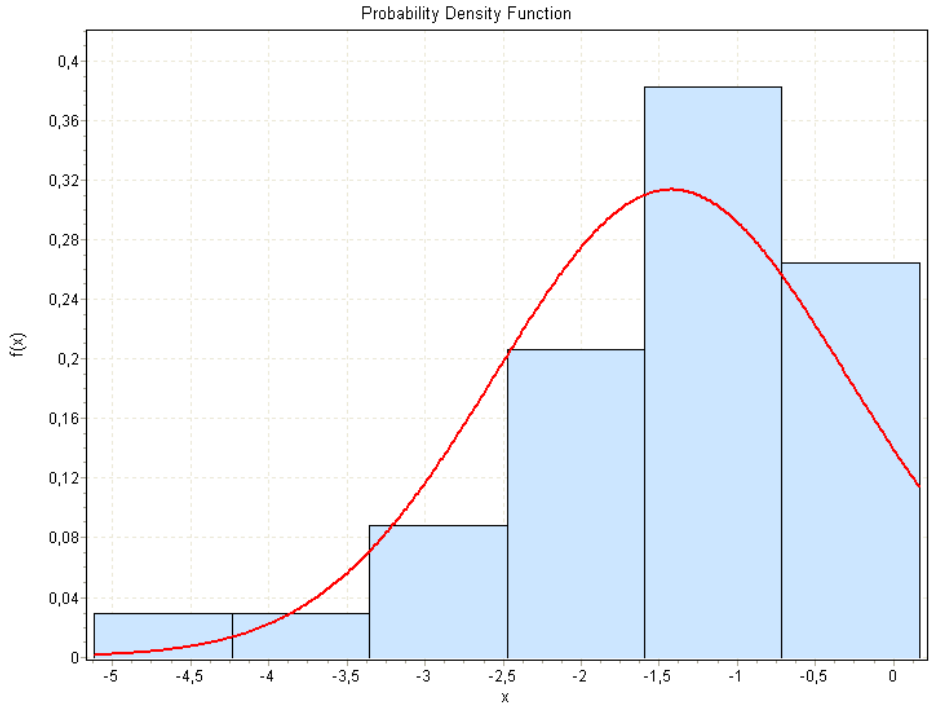

Kolmogorov-Smirnov					
Sample Size	34				
Statistic	0,12751				
P-Value	0,5935				
Rank	17				
α	0,2	0,1	0,05	0,02	0,01
Critical Value	0,17909	0,20472	0,22743	0,25429	0,27279
Reject?	No	No	No	No	No

Appendix 7 F-tests and t-tests

F test: test equality of variances

H0 hypothesis: variance of classes are equal

The F test is performed for all pairs of classes. There are seven classes which means there are 21 pairs of classes. If the p-value < 0.05, then reject H0: no equality of variances. A 5% critical area is applied.

Z-test: equality of means

H0 hypothesis: means of classes are equal

The Z-test is performed for all pairs of classes that have equal variances according to the F-tests. If the p-value < 0.05, then reject H0: no equality of means. A 5% critical area is applied.

Conclusion

The table below shows which pairs of classes have equal variances and equal means. A red cell means the H0 hypothesis is rejected during a F-test OR a Z-test. A green cell means that during both tests the H0 hypothesis is accepted.
The pairs with a green cell can be merged together if desirable. The pairs of classes that will be merged together are all the *Forest* classes and the *Golf* and *Lawn* classes.

CLASS	*AB Forest*	*C Forest*	*D Forest*	*Cropland*	*Grassland*	*Golf*	*Lawn*
AB Forest		F: Y T: Y	F: Y T: Y	F: N	F: Y T: N	F: Y T: Y	F: Y T: Y
C Forest			F: Y T: Y	F: N	F: Y T: N	F: Y T: Y	F: Y T: Y
D Forest				F: Y T: N	F: Y T: N	F: Y T: Y	F: Y T: Y
Cropland					F: Y T: N	F: Y T: N	F: N
Grassland						F: Y T: N	F: Y T: N
Golf							F: Y T: Y
Lawn							

F: N = Reject H0: no equality of variance. F: Y = Accept H0: equality of variance

Appendix 8 Measurement error of the saturated hydraulic conductivity

The measurement error is calculated for ten randomly chosen measurements.

Measurement no.	Error e as % of *Ksat*
15a	0.1587
24a	0.001339
38a	0.1646
45a	0.1673
46a	0.7848
51b	0.1308
53a	0.000157
69b	0.0567
73b	0.014
74a	0.0342
average	1.8075296

Appendix 9 Relation between slope and depression storage

Forest class

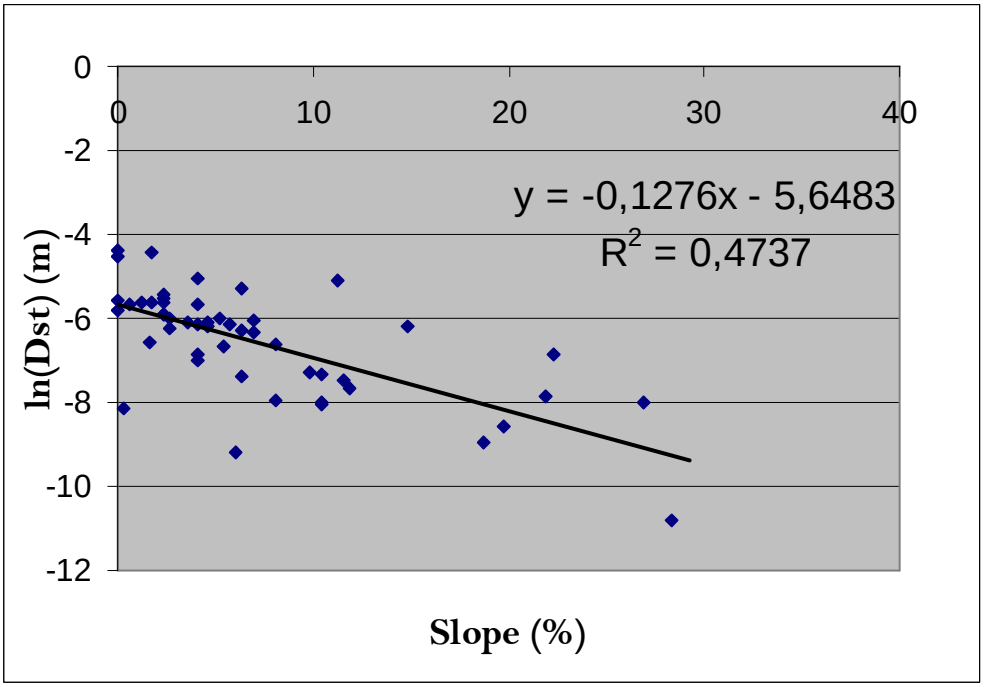

Cropland class

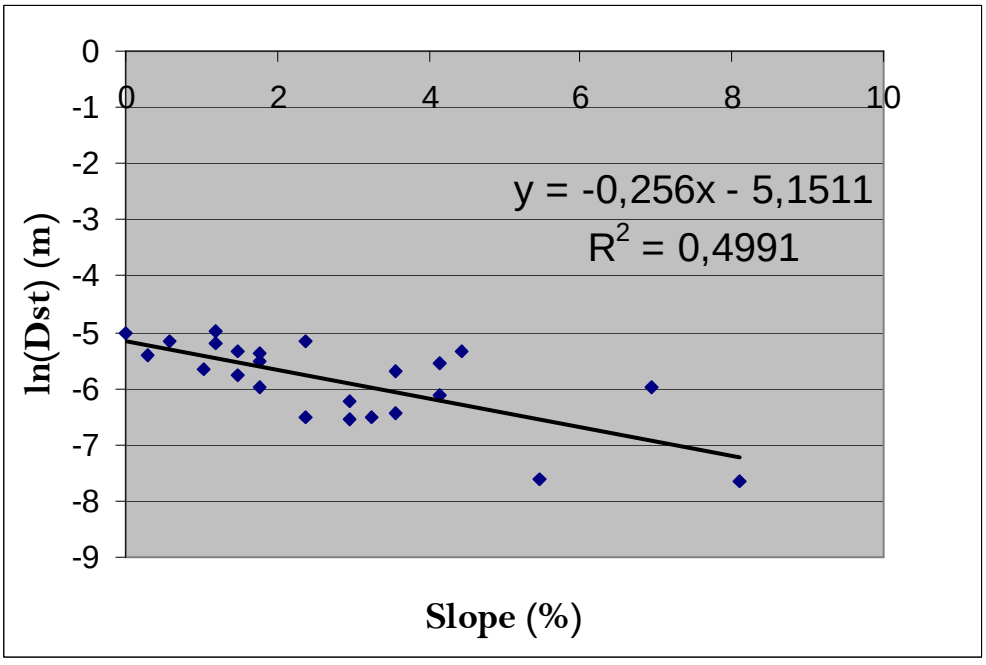

Grassland class

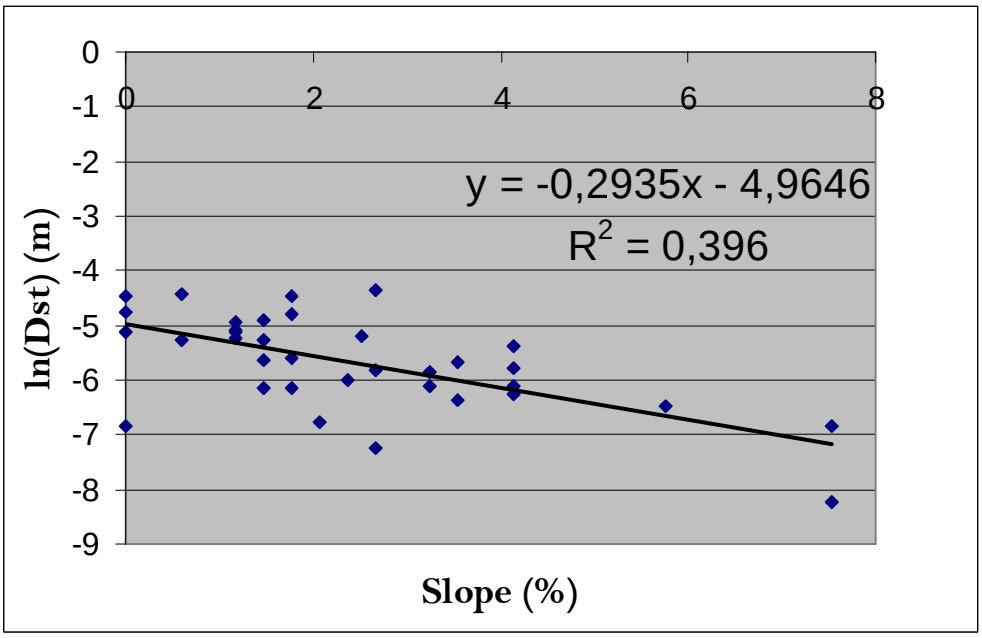

Golf/Lawn class

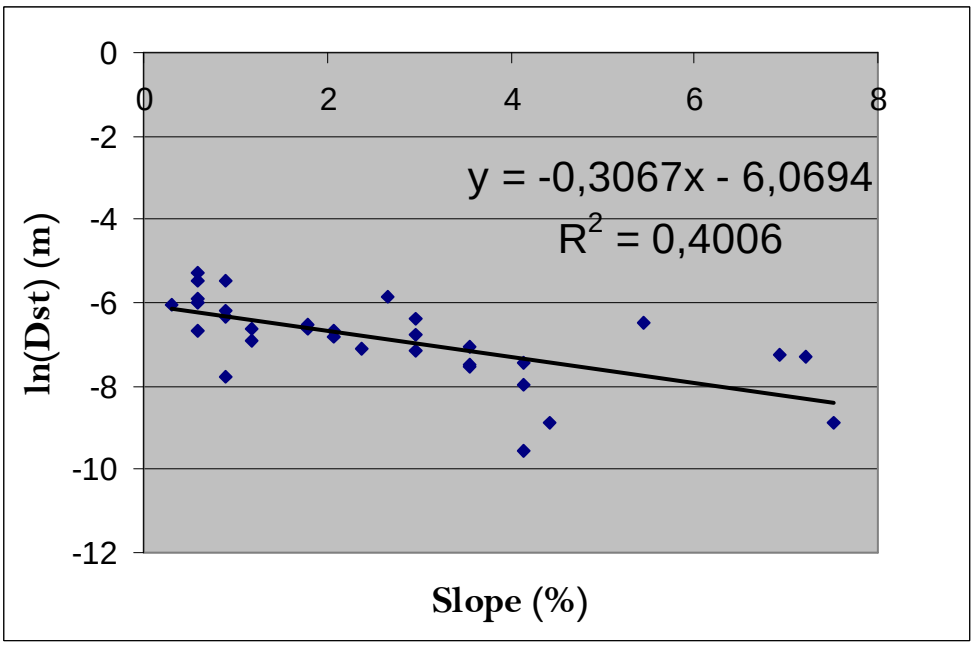

Appendix 10 Cumulative frequency distribution of both events

Cumulative frequency is on the y-axis and cumulative runoff (m^3) on the x-axis.

January 2010

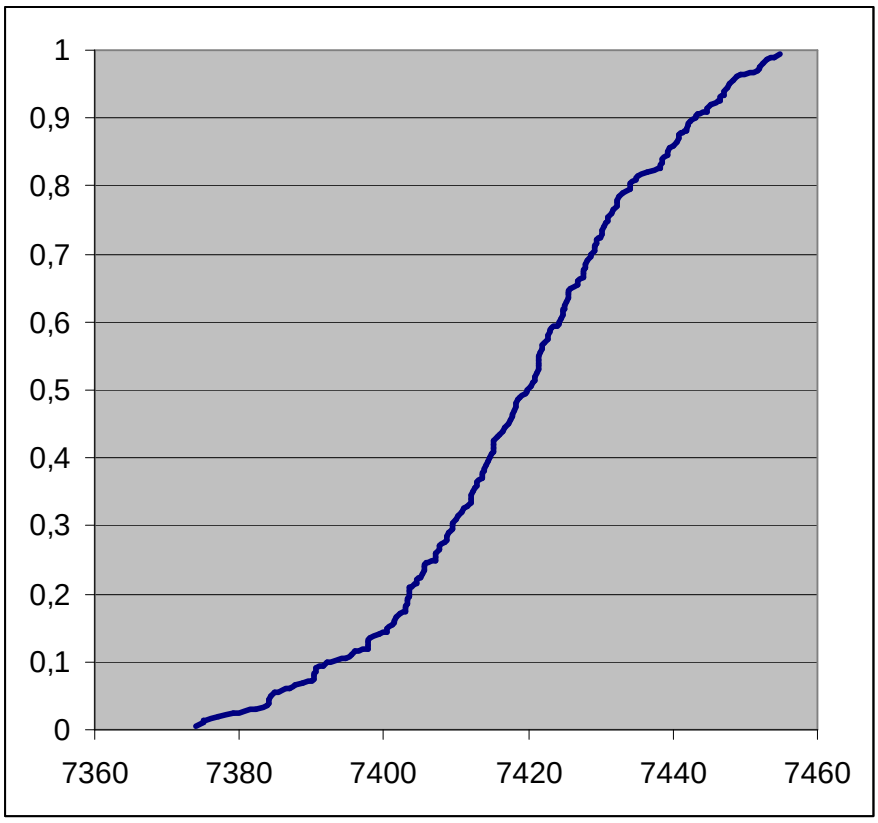

March 2010

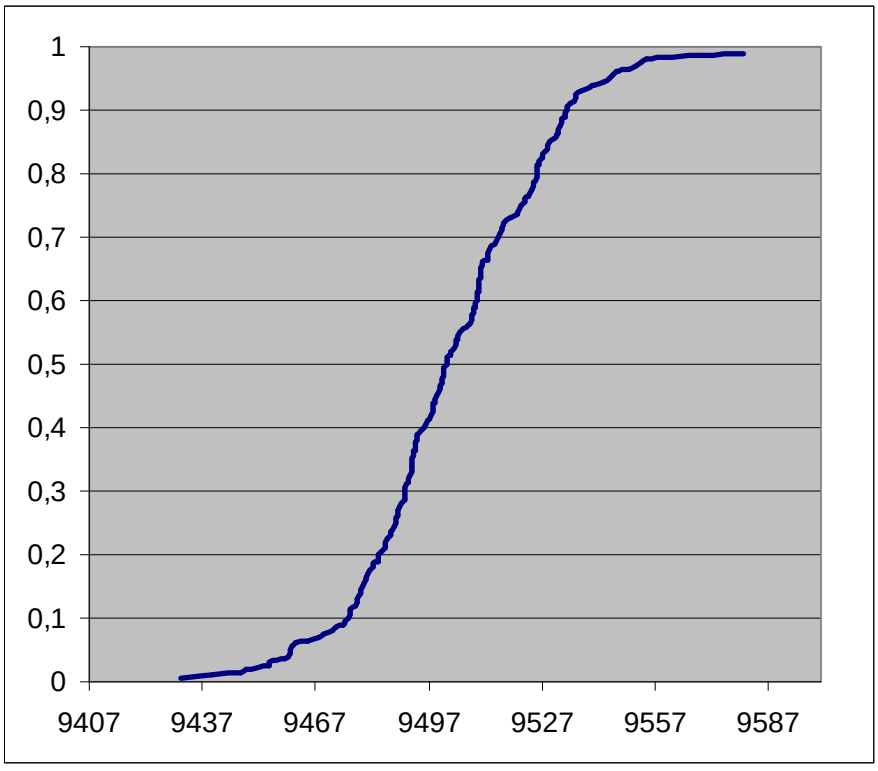

Appendix 11 Uncertainty in the cumulative runoff

Monte Carlo simulation yields 200 cumulative runoff curves for each event. They are plotted in one graph for each event, shown below. Cumulative runoff (m^3) is on the y-axis and timesteps (30 s) on the x-axis. The limited spreading of the curves is an indication of the small uncertainty of the model.

January 2010

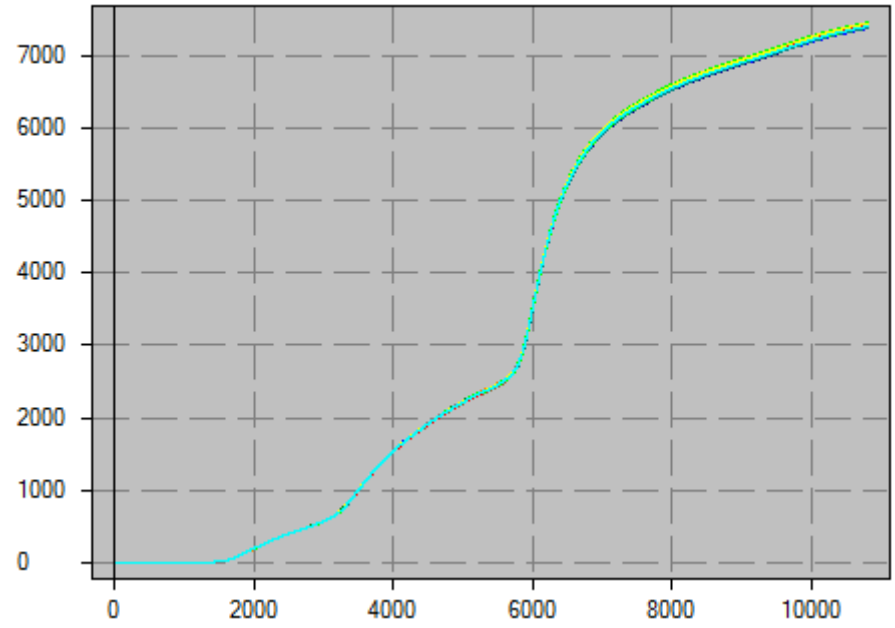

March 2010

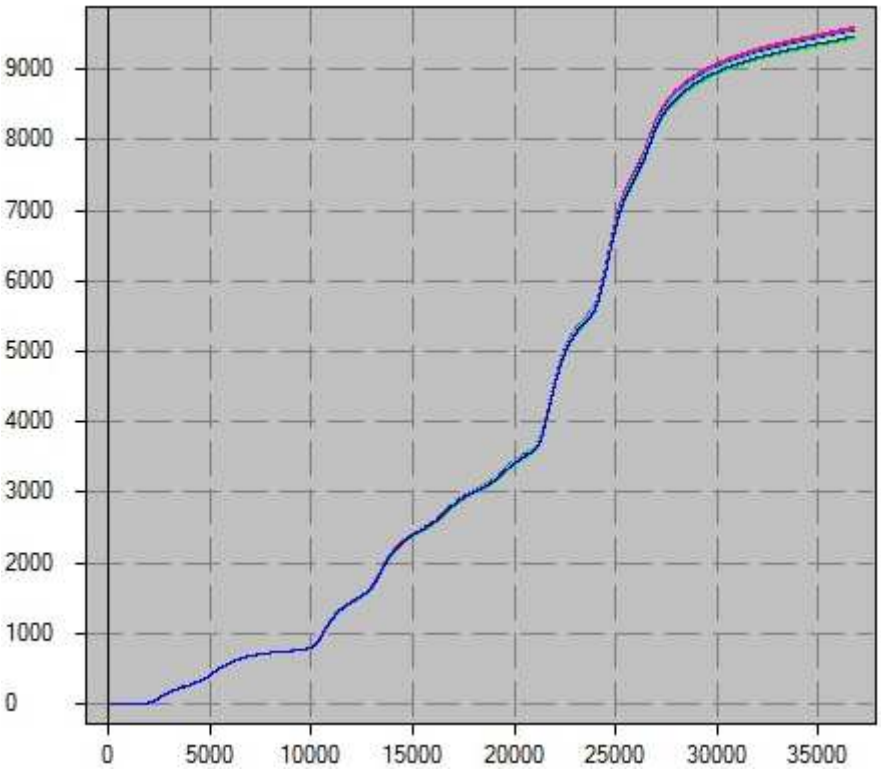

Appendix 12 PCRaster model script

```
# Rainfall-runoff model for the Disappearing Lake catchment, Marcellus, NY, USA
# Kees van der Hoorn, Koen Berendsen
# University Utrecht February 2010
#!--lddin

binding
##RAIN-##INTERCEPTION
T=scalar(30); #duration of a timestep(seconds)
Clone=input\clone.map; #mask showing the catchment(boolean)
PrecipitationTSS=input\jan2010.tss; #timeseries with rainfall per timestep (m/timestep)

##GENERAL
LandUseKs=input\landuse.map; #map representing units with different infiltration capacity
Dem=input\dem.map; #elevation model (m)

##ROUTING
Ldd=results\ldd2.map; #local drain direction map
Ang=scalar(0); #map with the angle of channel borders (deg)
Beta=scalar(0.6); #Beta.map; #map with the Beta routing parameter for every cell 0.6
Sinkhole=results\Sinkhole2.map; #map with the location of the sinkhole used as outflow
points/pits
Slope= input\slope.map; # contains new slope map

##OUTPUT MONTE CARLO SIMULATION
DepressionStore=results\depstore.map; #reported map with potential depression storage
(m)
KsT=results\Ks.map; #reported map with saturated conductivity (m/timestep)
lnKs=results\Ksln.map; #reported map with ln of the saturated conductivity (m/d)
B=resultss\B.map; #reported map with the integral capillary and saturation deficit
parameter B(m)
Runoff=results\runoffmarch.tss; #reported timeseries showing the sum of runoff of the
sinkhole (m3/timestep)
CumRunoff=results\cumrunoff.tss; #reported timeseries showing the cumulative runoff
(m3/timestep)
Floodvol=resultssens\floodvol.map;

areamap
Clone;

timer
1 10800 1;

initial
clone= boolean(LandUseKs);
COV= lookupscalar(input\avgCOV.txt, LandUseKs);
IntStM= lookupscalar(input\inter.txt, LandUseKs);
KsAve= lookupscalar(input\avgKs.txt,LandUseKs);
KsStdev= lookupscalar(input\stdKs.txt, LandUseKs);
Saturated= lookupscalar(input\saturated.txt, LandUseKs);
ROC= lookupscalar(input\avgROC.txt, LandUseKs);
```

```
N=lookupscalar(input\manN.txt, LandUseKs);
Upstream =accuflux(Ldd,1);
Bw=lookupscalar(input\stream.txt, Upstream);
Stream = if(Bw==10,0,1);

##RAIN##INTERCEPTION
#initial cumulative rain (m)
RainCum=scalar(0);
#set the interception store to initial content(m)
IntSt=scalar(0);

##INFILTRATION
#Random number from a normal distribution with mean 0 and stdev 1
RandomStdev1=normal(Clone);
#include saturated areas in KsAve and KsStdev
KsAve=if(Saturated==1, scalar(-200), KsAve);
KsStdev=if(Saturated==1, scalar(0), KsStdev);
#ln of Saturated conductivity (Ks in m/d)
lnKs=KsAve+RandomStdev1*KsStdev;
#Saturated conductivity m/timestep
KsT=exp(lnKs)/(24*60*60)*T;
#B determined by the empirical relation Ks vs B (m)
B=min(max(exp(0.991*lnKs-scalar(1.7932)+normal(Clone)*sqrt(2.793076431
*(1+1/146+((scalar(lnKs)-0.8081997)**2)/356.7421316))),0.00000000001),5);
#water deficit parameter including rocks (m)
BRock=B*(1-ROC);
#initial ponded water (m)
Pond=scalar(0);
#Initial actual infiltration (m/timestep)
FcA=scalar(0.0000000001);
#initial cumulative infiltration (m)
FCum=if(Clone,scalar(0));
#-slope set to small value

##DEPRESSION STORAGE
#empirical relations for effective depression storage for different land use types as a function
of slope
Forest= exp((-0.1276*scalar(Slope)-5.6483)+normal(Clone)*sqrt(1.67562022*(1+1/
54+((scalar(Slope)-8.52518519)**2)/3752.378548)));
Cropland= exp((-0.2935*scalar(Slope)-4.9646)+normal(Clone)*sqrt(0.772313*(1+1/
35+((scalar(Slope)-2.424)**2)/120.6946)));
Grassland= exp((-0.256*scalar(Slope)-5.1511)+normal(Clone)*sqrt(0.537268*(1+1/
24+((scalar(Slope)-2.783333)**2)/94.13893)));
GolfLawn= exp((-0.3067*scalar(Slope)-6.0694)+normal(Clone)*sqrt(0.977949*(1+1/
32+((scalar(Slope)-2.669063)**2)/129.0695)));

#calculates the depression storage (m) per land use type
depstore=if(LandUseKs==2,Forest, if(LandUseKs==4,Forest,
if(LandUseKs==5,Cropland, if(LandUseKs==6, Grassland, if(LandUseKs==3, GolfLawn,
if (LandUseKs==1 or LandUseKs==7 or LandUseKs==8, scalar(0.000000000001)))))));
DepressionStore= if(depstore>0.05,0.05,depstore);
```

```
#initial depression storage
Dst=scalar(0.00000000001);

##ROUTING
#term for alpha
AlphaTerm=(N/sqrt(Slope))**Beta;
#power for Alpha
AlpPow=(2/3)*Beta;
#initial water height (m)
H=scalar(0.00000000001);
#initial approximation for alpha
P=if(Stream==1, Bw+2*H,Bw);
# alpha term
Alpha=if(Clone,AlphaTerm*(P**AlpPow));
#initial stream flow (m3/s)
Q=if(Clone,scalar(0.00000000000000001));
#initial volume of runoff water (m3)
Q_V=scalar(0.00000000000000001);

#initial cumulative numbers
CumRunoff=scalar(0);
RainNetTOT=scalar(0);
FcATOT=scalar(0);
DstTOT=scalar(0);

#cell data
CL= celllength();
DCL= if(Ldd ne 5,downstreamdist(Ldd)*CL,CL);
CA= CL**2;

#Lake volume
Floodvol= maptotal(CA*abs(if(Dem<198.7,Dem-198.7)));

dynamic

##RAIN-##INTERCEPTION
#rain m/timestep
Rain=timeinputscalar(PrecipitationTSS,Clone);
#cumulative rain (m)
RainCum=RainCum+Rain;
#intercepted water, spreaded over grid cell(m)
Int=Rain*COV;
#interception store for area covered, previous timestep (m)
IntStOld=IntSt;
#interception store for area covered (m)
IntSt=if(IntStM>0,IntStM*(1-exp(-RainCum/IntStM)),0);
#flux to interception store for area covered (m/timestep)
ToIntSt=IntSt-IntStOld;
#flux to interception store for whole cell (m/timestep)
ToIntStC=ToIntSt*COV;
#leaf drip(m)
LD=Int-ToIntStC;
```

```
#total net rain per timestep for whole cell (m/timestep)
RainNet=Rain-Int+LD;
# cumulative rain reaching ground. total rain-this number=intercepted water

##INFILTRATION
#water on surface as runoff of the previous timestep m
Qsurf=Q_V/CA;
#water on surface available for infiltration (m);
SurfW=if(Stream==1,RainNet+Dst,RainNet+Dst+Qsurf);
#exponent of Smith and Parlange
ExpFB=exp(min(FCum/BRock,30));
#potential infiltration (m/timestep)
Fc=KsT*(ExpFB/max((ExpFB-1),0.000000000001));
#actual infiltration(m/timestep)
FcA=if(SurfW gt Fc,Fc,SurfW);
#cumulative infiltration (m);
FCum=FCum+FcA;
#water on surface after infiltration (m);
Pond=max(SurfW-FcA,0);

##DEPRESSION STORAGE
#Amount of water in surface storage (m)
Dst=if(Pond gt DepressionStore, DepressionStore, Pond);
#Flux of excess water (m/timestep) going in or out the Routing model
#(could be negative for cells where part of Qsurf has infiltrated or filled the Dst)
ExcessW=if(Stream==1,max(Pond-Dst,0), max(Pond-Dst,0)-Qsurf);

##ROUTING
#Excess water multiplied by cell area and timestep to convert to (m3/s)
QIn=ExcessW*CA/T;
#lateral inflow per distance along stream ((m3/s)/m)
q=QIn/DCL;
#discharge (m3/s)
Q=kinematic(Ldd,Q,q,Alpha,Beta,1,T,DCL);
#water depth (m)
A=Alpha*Q**Beta;
H=(Alpha*(Q**Beta))/Bw;
#wetted perimeter
P=if(Stream==1,Bw+2*(H/cos(Ang)),Bw);
#Alpha
Alpha=AlphaTerm*(P**AlpPow);
#flow velocity (m/s)
V=Q/A;
#volume of runoff water in raster cell (m3)
Q_V=Q*(DCL/V);

##OUTPUT
# the sum of the runoff that reached the sinkhole (m3/timestep)
report Runoff=maptotal(if(Sinkhole,Q*T,0));
# cumulative total runoff (m3)
report CumRunoff=CumRunoff+Runoff;
```